J. Fluid Mech. (2001), *vol.* 441, *pp.* 31–65. Printed in the United Kingdom

On a class of unsteady, non-parallel, three-dimensional disturbances to boundary-layer flows

By PETER W. DUCK AND SONIA L. DRY

Department of Mathematics, University of Manchester, Manchester M13 9PL, UK

(Received 13 July 1999 and in revised form 5 February 2001)

Steady, spatial, algebraically growing eigenfunctions are now known to occur in several important classes of boundary-layer flow, including two-dimensional hypersonic boundary layers and more recently in Blasius boundary layers subject to three-dimensional linearized disturbances, and in more general three-dimensional boundary layers. These spatial eigensolutions are particularly important and intriguing, given that they exist within the broad limits of the classical steady boundary-layer approximation, and as such are independent of Reynolds number.

In this paper we make the natural extension to these previous (stability) analyses by incorporating the effects of unsteadiness into the model for treating disturbances to a quite general class of similarity-type boundary-layer flows. The flow disturbances are inherently non-parallel, but this effect is properly incorporated into the analysis.

A further motivation for this paper is that Duck *et al.* (1999, 2000) have shown that by permitting a spanwise component of flow within a boundary layer of the appropriate form (in particular, growing linearly with the spanwise coordinate), it is found that new families of solutions exist – even the Blasius boundary layer has a three-dimensional 'cousin'. Therefore a further aim of this paper is to assess the stability of the different solution branches, using the ideas introduced in this paper, to give some clues as to which of the solutions may be encountered experimentally.

Several numerical methods are presented for tackling various aspects of the problem. It is shown that when algebraically growing, steady eigensolutions exist, their effect remains important in the unsteady context. We show how even infinitesimal, unsteady flow perturbations can provoke extremely large-amplitude flow responses, including in some cases truly unstable flow disturbances which grow algebraically downstream without bound in the linear context. There are some interesting parallels suggested therefore regarding mechanisms perhaps linked to bypass transition in an important class of boundary-layer flows.

1. Introduction

Great strides have been made in recent decades in understanding various boundary-layer transition processes. At high Reynolds numbers we have quite a good understanding and description of the formation of Tollmien–Schlichting waves and of the earlier stages of the associated transition process, due in part to multi-layered asymptotic analysis (Smith 1979*a*, *b* for example). A quite recent, comprehensive summary of work in this area can be found in Cowley & Wu (1994).

At finite Reynolds numbers, in addition to direct numerical simulations (for example

Rist & Fasel 1995), the parabolized stability equations (Bertolotti 1991; Herbert & Lin 1993) provide a rapid and reliable means of flow analysis, including non-parallel effects due to boundary-layer growth, albeit using a procedure which strictly is non-rational (not all the stages in the procedure can be fully justified from a strict, theoretical standpoint).

Luchini (1996) found that algebraic growth within a Blasius boundary layer is possible, with spanwise periodic disturbances (of large wavelength compared with the boundary-layer thickness). Duck, Stow & Dhanak (1999, 2000) showed how such growth occurs within a broad range of three-dimensional boundary layers, subject to disturbances that grow linearly in the spanwise direction. Indeed this type of phenomenon is not completely new, but was found some time ago in certain types of hypersonic boundary layers by Neiland (1970), Mikhailov *et al.* (1971) and Brown & Stewartson (1975). It was suggested by Luchini (1996) that this mechanism is a good candidate for bypass transition. The area of 'algebraic' growth of disturbances has been the subject of quite detailed study in recent times, starting principally with Landahl (1980), and followed by Hultgren & Gustavsson (1981), Butler & Farrell (1992), Reddy & Henningson (1993), Trefethen *et al.* (1993), and others. There is now much evidence that three-dimensional perturbations can provoke a significantly different response inside a two-dimensional boundary layer than two-dimensional flow perturbations, in contrast to the classical result of Squire (1933). Two very recent papers on the linear, algebraic growth within Blasius boundary layers by Andersson, Berggren & Henningson (1999) and Luchini (2000) have extended the earlier ideas of Luchini (1996) to disturbances of wavelengths comparable with the boundary-layer thickness. Of particular interest in these studies is the concept of optimal perturbations, i.e. determining the initial perturbations that lead to the maximum energy growth. Andersson *et al.* (1999) and Luchini (2000) also showed that this maximum growth was achieved at a finite spanwise wavenumber (based on the boundary-layer thickness).

The non-parallel nature of most boundary-layer flows further complicates matters, and has also been the subject of much attention, and indeed controversy. Leaving aside direct numerical simulations already mentioned (which undoubtedly do have an important role to play, although at some computational cost), several approaches have been adopted to treat these effects. One approach was followed by Barry & Ross (1970) and Chen, Sparrow & Tsou (1971) and leads to a form of the Orr–Sommerfeld equation. A second, more successful approach was that of Bouthier (1972, 1973) and Saric & Nayfeh (1975), although again this approach is not completely justifiable from the strict theoretical point of view. The aforementioned parabolized stability equations can of course also treat non-parallel effects, and indeed the downstream development of the flow is a key element of this technique.

One aim of this paper is to extend the work of Luchini (1996) and of Duck *et al.* (1999, 2000) to include unsteady effects. These significantly alter the nature of the flow response, and also lead naturally to several of the ideas and concepts mentioned above, including transient/algebraic growth and non-parallel flow effects, flow processes that to a degree become intermingled in problems of this type. Luchini (2000) does present some unsteady results for his class of perturbation to the Blasius boundary layer, in particular showing that the maximum energy growth/optimal disturbances occur at zero frequency. In the present paper we are able to show that for our class of problem, the zero-frequency case is somewhat special (certainly it may be regarded as a singular limit for our class of disturbance).

In Dhanak & Duck (1997) and Duck *et al.* (2000) it was shown that for free-stream

flows of the form x^n (x being a measure of distance from some leading edge, at which the boundary layer first forms), in addition to the classical Falkner–Skan (Rosenhead 1966) class of self-similar boundary-layer flows, the three-dimensional boundary-layer equations also admit three-dimensional, similarity-type solutions, which involve a crossflow component that grows linearly in the crossflow direction, even if the imposed conditions do not explicitly force crossflow effects (the two other velocity components are taken to be independent of the crossflow coordinate); even Blasius flow has a three-dimensional 'cousin' (Dhanak & Duck 1997). It is of course well known that the two-dimensional Falkner–Skan problem exhibits dual solutions when $n < 0$ (Hartree 1937), with the additional solution exhibiting reversed flow. Craven & Peletier (1972) and Oskam & Veldman (1982) have found additional Falkner–Skan-type solutions at extreme values of n, although these are generally oscillatory in nature; we conclude therefore that the nature of these additional solutions suggests they will be difficult to observe experimentally. On the other hand, the three-dimensional, additional solutions of Dhanak & Duck (1997) and Duck *et al.* (2000) are relatively benign in nature, with the crossflow velocity component generally taking on a jet-like profile.

At this point it is probably worth raising the issue of the growth of the crossflow velocity component in the spanwise direction, z. This obviously becomes unbounded as $|z| \to \infty$; certainly one interpretation of the solution is that it represents a local solution behaviour (in powers of z, as $z \to 0$), very much in the same way as Hiemenz flow (which itself becomes unbounded as $|x| \to \infty$), is generally regarded as a localized solution about an attachment point. Nonetheless, in the present analysis there is no requirement that z be necessarily small. It is not our intention here to consider the more global nature of the flow field, which would inevitably involve a full discussion of the inviscid flow region (together with probably other viscous zones), thereby losing the generic nature of the study. Rather we focus our attention on what may be regarded as a generic problem involving a fully viscous boundary layer that admits solutions of the aforementioned class.

We will study the effects of unsteady perturbations on general boundary-layer flows possessing the spanwise behaviour just described and hence this work is also applicable to the classical set of two-dimensional, self-similar, boundary-layer flows. The disturbances to the flow are taken to be of the same form as the basic flow, i.e. with a spanwise velocity component that grows linearly with the spanwise coordinate, the other two velocity components being independent of this direction. The analysis is fully rational, insofar as all steps can be justified on the basis of infinite Reynolds number theory; as such, our analysis leads to Reynolds number independent results. A further aim of this paper (in the light of the points raised above) is to attempt to shed some light on to which of the various possible solutions are likely to be observed experimentally, utilizing stability arguments of the class under consideration.

The outline of the paper is as follows. In § 2 we formulate the problem, including defining the class of base states we consider and also the nature of the flow perturbations. In § 3 the special case '$n = 1$' is considered, which corresponds to the stagnation point flow, in which it has been shown (Davey & Schofield 1967; Schofield & Davey 1967; Duck *et al.* 2000) that two solutions can exist, the first being the well-known two-dimensional solution of Hiemenz (Rosenhead 1966), the second a three-dimensional flow. For this choice of n a good deal of simplification is possible, since the perturbation equations can be shown to lose their streamwise spatial dependence, and even the effects of nonlinear perturbations are relatively straightforward to analyse. In § 4, the effects of an impulsive perturbation on the boundary layer (for general values of the velocity parameter n) are considered; in this

case the similarity form is not applicable to the flow perturbations, and consequently there is a significant complication to the analysis and solution. In cases where steady, leading-edge eigenstates exist (see above), the computation of unsteady perturbations proves difficult. This leads to § 5, involving temporally periodic flow perturbations, which are fully analysed. On the basis of this work, a spectral method is developed which overcomes certain of the numerical difficulties found in § 4. In § 6 a further class of spatio-temporal flow perturbation is discussed, which sheds further light on the results of § 5 (and some of the difficulties encountered in § 4). Our concluding discussion may be found in § 7.

2. Formulation

Consider the classical three-dimensional, unsteady, incompressible boundary-layer formulation. We take $L(x, y, z)$ to be the orthogonal, dimensional coordinates, where L is some reference lengthscale (defined, typically, by the spatial scale of the free-stream velocity variation), and where x is measured in the direction of the free stream, y is measured normal to a (flat) surface, which lies in $y = 0$, $x > 0$; dimensional time is written $(L^2/\nu)t$, ν being the kinematic viscosity. The corresponding velocity components (non-dimensionalized with respect to the typical free-stream velocity U_∞) are then written

$$u = U^*(x, Y, z, t), \quad v = Re^{-1/2} V^*(x, Y, z, t), \quad w = W^*(x, Y, z, t). \tag{2.1}$$

Here we have set $Y = Re^{1/2} y$ to be the usual boundary-layer coordinate, where the Reynolds number $Re = U_\infty L/\nu$, which is taken to be large throughout. The standard (classical) boundary-layer equations may then be written in the form

$$U^*_t + U^* U^*_x + V^* U^*_Y + W^* U^*_z = U^*_{YY} - P^*_x, \tag{2.2}$$

$$W^*_t + U^* W^*_x + V^* W^*_Y + W^* W^*_z = W^*_{YY} - P^*_z, \tag{2.3}$$

$$U^*_x + V^*_Y + W^*_z = 0, \tag{2.4}$$

$$P^*_Y = 0. \tag{2.5}$$

The dimensional pressure has been written $\rho_\infty U^2_\infty P^*$, ρ_∞ being the density of the (incompressible) fluid. Following the recent work of Duck *et al.* (1999, 2000), we now seek solutions to this set of equations in the form

$$U^* = \hat{U}(x, Y, t), \tag{2.6}$$

$$V^* = \hat{V}(x, Y, t), \tag{2.7}$$

$$W^* = z\hat{W}(x, Y, t), \tag{2.8}$$

$$P^* = P(x, t). \tag{2.9}$$

This obviously restricts the class of flows to be considered, but nonetheless the resulting class is important from a practical (as well as theoretical) point of view. In particular (2.6)–(2.9) above assume the following:

(i) a linear increase of the crossflow in the crossflow direction (z);
(ii) independence of the other velocity components of the crossflow direction;
(iii) independence on the pressure of z, implying that the crossflow velocity vanishes outside the boundary layer (i.e. in the free stream).

Some discussion of this class of flow (and its significance) has already been given in

the previous section, but it does encompass a wide range of boundary-layer flows (including all the two-dimensional classical boundary-layer flows).

To proceed we introduce a new set of dependent and independent variables as follows:

$$\hat{U} = x^n U(\xi, \eta, t), \tag{2.10}$$

$$\hat{V} = \frac{x^{(n-1)/2}}{\sqrt{2}}[(1-n)\eta U - \Phi], \tag{2.11}$$

$$\hat{W} = \frac{x^{n-1}}{\sqrt{2}} W = \frac{x^{n-1}}{2}[(1-n)U - \Psi], \tag{2.12}$$

where

$$\eta = \frac{Y}{\sqrt{2}\xi}, \tag{2.13}$$

$$\xi = x^{(1-n)/2}. \tag{2.14}$$

It is also useful (as in Duck *et al.* 1999, 2000) to introduce a modified vorticity function, namely

$$\theta = \Psi_\eta. \tag{2.15}$$

The quantities $\Phi(\xi, \eta, t)$ and $\Psi(\xi, \eta, t)$ may be regarded as forms of vector potential. In terms of these new variables, the boundary-layer equations (2.2)–(2.5) may be written in the form

$$U_{\eta\eta} + 2nf^2 + \xi(1-n)ff_\xi + 2\xi^2 f_t - 2\xi^2 U_t + \Phi U_\eta - \xi(1-n)UU_\xi - 2nU^2 = 0, \tag{2.16}$$

$$2U + (1-n)\xi U_\xi = \Phi_\eta + \Psi, \tag{2.17}$$

$$\theta_{\eta\eta} - 2(1-n^2)UU_\eta + \Phi\theta_\eta + \Psi\theta + 2U\theta - 2\xi^2\theta_t + (n-1)\xi[-\theta U_\xi + U\theta_\xi + \Psi_\xi U_\eta] = 0, \tag{2.18}$$

together with (2.15). The free-stream conditions are that

$$U \to f(\xi, t), \qquad \Psi \to (1-n)f(\xi, t), \qquad \theta \to 0 \tag{2.19}$$

as $\eta \to \infty$. The condition on Ψ ensures zero crossflow velocity in the free stream, whilst $f(\xi, t)$ denotes the streamwise and temporal variation of the free stream. The free-stream condition for Φ may be deduced from (2.17) together with (2.19), leading to

$$\Phi_\eta \to (1+n)f + (1-n)\xi f_\xi \tag{2.20}$$

as $\eta \to \infty$; this condition was generally utilized explicitly in our numerical scheme, since it was found beneficial to work with the η-differentiated form of (2.17), i.e. a second-order equation for Φ.

It is possible to combine (2.15) with (2.18), and then to integrate with respect to η, to eliminate θ, and this leads instead to the equation

$$\Psi_{\eta\eta} - (1-n^2)U^2 + \Phi\Psi_\eta - 2\xi^2\Psi_t + \Psi^2 + (n-1)\xi U\Psi_\xi = -2\xi^2(1-n)f_t + 2n(n-1)f^2 - (n-1)^2\xi ff_\xi, \tag{2.21}$$

which offers some advantages over the previous system, and is employed later. It is

important to note that for two-dimensional flows (for which $\hat{W} \equiv 0$), then

$$\Psi = (1-n)U, \tag{2.22}$$

$$\theta = (1-n)U_\eta, \tag{2.23}$$

in which case it is possible to show that (2.18) is entirely consistent with (2.16), even when the solution is dependent on ξ and t and is nonlinear. In Duck *et al.* (2000) a detailed study of steady, *similarity* solutions to the problem, corresponding to

$$\hat{U} = x^n U_0(\eta), \quad \hat{V} = x^{(n-1)/2} V_0(\eta), \quad \hat{W} = \frac{x^{n-1}}{\sqrt{2}} W_0(\eta) \tag{2.24}$$

was made; the governing system in this case is (2.15)–(2.18), with $\xi = 0$. Figure 1 shows distributions of these similarity base-flow states taken from the study of Duck *et al.* (2000), in particular the variations of $U_{0\eta}(0)$, $W_{0\eta}(0)$, $\theta_0(0)$ with the similarity parameter n. The $W_0(\eta) \equiv 0$ solutions correspond to the familiar Falkner–Skan family of solutions (Rosenhead 1966), whilst the additional solutions are three-dimensional in nature. The significance of the dashed lines will be explained shortly, but at this stage they serve as a useful means of correlating the three distributions shown in figure 1. Note also the (small) solution branch close to $n = 0-$, making a total of six solutions in this regime of n.

In Duck *et al.* (2000) steady spatial perturbations to the above similarity states were considered (following on from the work of Duck *et al.* 1999). In particular it is found that standard, parabolic downstream-marching techniques, as commonly employed in boundary-layer computations are, more often than not, inappropriate for problems of this type; the reason for this can be illustrated as follows. Suppose we take one of the basic similarity states as detailed above. We then seek linearized eigensolutions close to the leading edge as follows (an approach similar to that devised by Libby & Fox 1963; Chen & Libby 1968):

$$\left.\begin{aligned} U(\xi,\eta) &= U_0(\eta) + \xi^\lambda \tilde{u} + \cdots, \quad \Phi(\xi,\eta) = \Phi_0(\eta) + \xi^\lambda \tilde{\phi} + \cdots, \\ \Psi(\xi,\eta) &= \Psi_0(\eta) + \xi^\lambda \tilde{\psi} + \cdots, \quad \theta(\xi,\eta) = \theta_0(\eta) + \xi^\lambda \tilde{\theta} + \cdots. \end{aligned}\right\} \tag{2.25}$$

In the above it is assumed that $\mathrm{Re}\{(1-n)\lambda\} > 0$ for consistency, such that the perturbation is small compared with the basic state. Substitution of these into (2.15)–(2.18), discarding the unsteady terms: leads to the following system determining the perturbation quantities:

$$2\tilde{u} + (1-n)\lambda\tilde{u} = \tilde{\phi}_\eta + \tilde{\psi}, \tag{2.26}$$

$$\tilde{u}_{\eta\eta} = 4nU_0\tilde{u} + \lambda(1-n)U_0\tilde{u} - \tilde{\phi}U_{0\eta} - \tilde{u}_\eta\Phi_0, \tag{2.27}$$

$$\tilde{\theta} = \tilde{\psi}_\eta, \tag{2.28}$$

$$\begin{aligned} \tilde{\theta}_{\eta\eta} - 2(1-n^2)[U_0\tilde{u}_\eta + \tilde{u}U_{0\eta}] + \tilde{\theta}_\eta\Phi_0 + \theta_{0\eta}\tilde{\phi} + \tilde{\psi}\theta_0 + 2\tilde{u}\theta_0 + \Psi_0\tilde{\theta} + 2U_0\tilde{\theta} \\ +(n-1)\lambda\{-\theta_0\tilde{u} + U_0\tilde{\theta} + \tilde{\psi}U_{0\eta}\} = 0, \end{aligned} \tag{2.29}$$

subject to the boundary conditions

$$\tilde{u}(0) = \tilde{\phi}(0) = \tilde{\psi}(0) = 0, \quad \tilde{u}, \tilde{\psi}, \tilde{\theta} \to 0 \text{ as } \eta \to \infty. \tag{2.30}$$

Solution of this eigenvalue problem reveals that states with $\mathrm{Re}\{(1-n)\lambda\} > 0$ do exist, and basic flows which admit such states are indicated by broken lines in figure 1. The existence of these leading-edge eigenstates has important repercussions (as will be

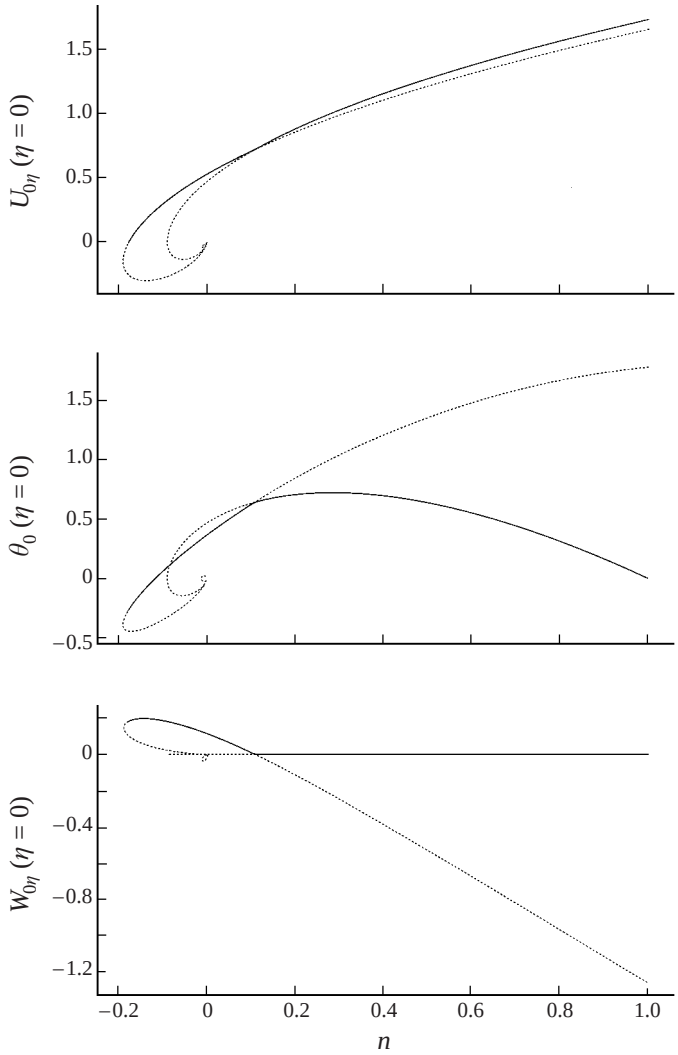

FIGURE 1. Base flow states.

seen later when considering unsteady disturbances) in addition to rendering standard parabolic marching schemes ill-posed (see below). As a result of performing a number of computations of this type on the base flows under consideration, it is possible to make the following general observations:

(i) At most only one solution exists with no values of λ such that $\mathrm{Re}\{(1-n)\lambda\} > 0$ for any value of n.

(ii) It is generally the solution with largest value of $U_{0\eta}(0)$ that has no values of λ such that $\mathrm{Re}\{(1-n)\lambda\} > 0$; witness the crossover at $n = 0.167\ldots$ where there is a changeover in the 'stability' of the solution branches. As n increases from below this value, the three-dimensional solution is initially 'stable' (or more precisely has no $\mathrm{Re}\{(1-n)\lambda\} > 0$), the two-dimensional solution branch is initially 'unstable' (or more precisely does have a $\mathrm{Re}\{(1-n)\lambda\} > 0$), and then there is a reversal of the 'stability' of these branches beyond this value of n.

(iii) Most (all ?) of the λ are real.

(iv) In regions of reversed flow in the streamwise direction ($U_{0\eta}(0) < 0$) many, probably an infinite number of, values of λ exist, such that $\mathrm{Re}\{(1-n)\lambda\} > 0$; this observation seems consistent with the problem being truly elliptic in these regions.

(v) It is worth pointing out that the quantity $(1-n)\lambda$ is more significant than λ *per se*, since the form ξ^{λ} translates into the physical coordinate as $x^{\lambda(1-n)/2}$, and so it is the quantity $(1-n)\lambda$ that actually controls the downstream development of the flow. It should be noted that $(1-n)\lambda$ remains finite as $n \to 1$.

From figure 1 (and Luchini 1996; Duck *et al.* 2000) we see that the familiar Blasius state does exhibit a positive value of λ. The existence of these steady eigensolutions obviously complicates the solution process, particularly those involving streamwise distributions of perturbation excitation, as considered by Duck *et al.* (1999), but they showed how such difficulties could be overcome using a quasi-elliptic approach to the problem, implementing downstream (in addition to upstream) conditions, just the sort of procedure that would be employed on an elliptic scheme, using second-order central differences. Under normal circumstances the dual specification of upstream and downstream conditions on a parabolic partial differential equation would obviously lead to an over-specified problem. The correctness of this approach however when the aforementioned steady, leading-edge eigenstates exist may be understood conceptually as follows, taking (to simplify the arguments) the linearized, steady disturbance system. A standard downstream marching procedure involving external forcing, of general form (including that described here), will lead inevitably to unbounded (algebraic) growth downstream. Assuming that the external forcing decays downstream, this growth downstream will be of the form ξ^{λ} (such computations have been performed by the authors and concur with this statement). The perturbation downstream therefore takes on the form of the growing eigensolution. Thus (recalling the linear nature of this problem) if we subtract off the appropriate 'amount' of eigensolution, we can achieve a state which has zero perturbation at the leading edge and decays downstream. The problem is strongly reminiscent of triple-deck/free-interaction problems (e.g. Stewartson & Williams 1969) in which an eigensolution exists which grows downstream; standard marching procedures based on the linearized version of problems of this type lead, in general, to exponentially growing downstream growth, but the addition of the correct 'amount' of eigensolution upstream (i.e. upstream influence) is sufficient to lead to a downstream-decaying solution. Equally, the two-dimensional supersonic, triple-deck problem is well known to be stable according to stability analyses (see for example Zhuk & Ryzhov 1978; Terent'ev 1978; Ryzhov & Zhuk 1980; Duck 1985). The 'quasi-elliptic' approach of Duck *et al.* (1999) may be regarded as an alternative to the 'eigensolution subtraction' technique described above, and automatically picks the coefficient of the leading-edge eigensolution to ensure downstream decay (when appropriate).

The recent interesting work of Andersson *et al.* (1999) and Luchini (2000) tackles an equally valid, related problem, from a different angle. Rather than studying the effects of a forcing, with a streamwise distribution, they determined the initial perturbation (used to trigger the flow disturbance) that leads to the maximum energy growth.

In this paper we shall be primarily concerned with small-amplitude, *unsteady* perturbations to similarity base flows of the type described above (see (2.24)). We therefore seek linearized unsteady spatially evolving solutions to the basic similarity states, writing

$$U = U_0(\eta) + \delta\tilde{u}(\eta, \xi, t) + \cdots, \tag{2.31}$$

$$\Phi = \Phi_0(\eta) + \delta\tilde{\phi}(\eta, \xi, t) + \cdots, \tag{2.32}$$

$$\Psi = \Psi_0(\eta) + \delta\tilde{\psi}(\eta, \xi, t) + \cdots, \tag{2.33}$$

$$\theta = \theta_0(\eta) + \delta\tilde{\theta}(\eta, \xi, t) + \cdots, \tag{2.34}$$

$$f = 1 + \delta\tilde{f} + \cdots, \tag{2.35}$$

where δ is a (small) amplitude parameter. The system governing the perturbation (tilde) quantities to leading order may then be written in the form (neglecting the $O(\delta^2)$ terms)

$$\tilde{u}_{\eta\eta} + 4n\tilde{f} + \xi(1-n)\tilde{f}_\xi + 2\xi^2\tilde{f}_t - 2\xi^2\tilde{u}_t + \tilde{\phi}U_{0\eta} + \Phi_0\tilde{u}_\eta - \xi(1-n)U_0\tilde{u}_\xi - 4nU_0\tilde{u} = 0, \tag{2.36}$$

$$2\tilde{u} + (1-n)\xi\tilde{u}_\xi = \tilde{\phi}_\eta + \tilde{\psi}, \tag{2.37}$$

$$\tilde{\theta} = \tilde{\psi}_\eta, \tag{2.38}$$

$$\tilde{\theta}_{\eta\eta} - 2(1-n^2)(U_0\tilde{u}_\eta + U_{0\eta}\tilde{u}) + \tilde{\phi}\theta_{0\eta} + \Phi_0\tilde{\theta}_\eta + \Psi_0\tilde{\theta} + \tilde{\psi}\theta_0 + 2U_0\tilde{\theta} + 2\tilde{u}\theta_0 - 2\xi^2\tilde{\theta}_t + (n-1)\xi[-\theta_0\tilde{u}_\xi + U_0\tilde{\theta}_\xi + \tilde{\psi}_\xi U_{0\eta}] = 0. \tag{2.39}$$

Note that (2.39) can usefully be replaced by

$$\tilde{\psi}_{\eta\eta} - 2(1-n^2)U_0\tilde{u} + \Phi_0\tilde{\psi}_\eta + \Psi_{0\eta}\tilde{\phi} - 2\xi^2\tilde{\psi}_t + 2\Psi_0\tilde{\psi} + (n-1)\xi U_0\tilde{\psi}_\xi = -2\xi^2(1-n)\tilde{f}_t + 4n(n-1)\tilde{f} - (n-1)^2\xi\tilde{f}_\xi. \tag{2.40}$$

The boundary conditions are then that

$$\tilde{u}(\eta = 0) = \tilde{\phi}(\eta = 0) = \tilde{\psi}(\eta = 0) = 0, \tag{2.41}$$

$$\tilde{u}(\eta \to \infty) \to \tilde{f}, \quad \tilde{\psi}(\eta \to \infty) \to (1-n)\tilde{f}, \quad \tilde{\theta}(\eta \to \infty) \to 0. \tag{2.42}$$

Notice here that the inclusion of unsteadiness inevitably results in spatial variations, on account of the multiplicative ξ^2 term that occurs in conjunction with the acceleration terms – the similarity form which exists for the steady base states is completely destroyed. We note that in the work related to (far-field) corner flows, Ridha (1992) considered a form of temporal, linear stability which amounts to the system (2.36)–(2.40), but with the spatial (ξ) terms neglected and with the ξ^2 term multiplying the time derivatives set equal to unity (in essence, amounting to a solution which is dependent on t/ξ^2 only). However, such a procedure, in general, cannot be justified from a rigorous point of view; but in the special case of $n = 1$ it turns out that a good deal of simplification occurs, even with the full nonlinear system (2.15)–(2.18). This case is considered in the following section; discussion of the other more general values of n is deferred until later.

3. The special case $n = 1$

As noted in the previous section, as $n \to 1$, the quantity $(1-n)\lambda$ remains bounded. However, for the special case of $n = 1$ we may study an alternative class of disturbance by means of merely setting $n = 1$ in (2.15)–(2.18), which leads to a problem where the ξ-derivatives may be neglected because of the $(1-n)$ factor. In the resulting system, since ξ only appears as a multiplicative factor on the acceleration terms, we may take $\xi = 1$ without any loss of generality, equivalent to considering perturbations which are dependent on t/ξ^2 (only), thereby reducing the dimension of the problem by one.

Indeed, this is related to the class of disturbance considered in § 6 for general values of n.

When $n = 1$, the two base states are the well-known two-dimensional Hiemenz solution (Rosenhead 1966) whilst the three-dimensional solution corresponds to that found and discussed by Davey & Schofield (1967) and Schofield & Davey (1967). The effects on both solutions of a nonlinear, unsteady perturbation in the free stream may be studied, which we carried out by means of the following free-stream behaviour for the streamwise velocity:

$$f(t) = 1 + \gamma t \mathrm{e}^{-t}, \tag{3.1}$$

corresponding to a perturbation which grows from the undisturbed state ($f(0) = 1$) and then ultimately decays back to this undisturbed state; γ represents the amplitude of the flow perturbation, $\gamma > 0$ representing an initial flow acceleration, followed by a retardation, $\gamma < 0$ representing an initial flow retardation, followed by an acceleration. The system was then solved using a second-order Crank–Nicolson method in t, together with a second-order, central, finite-differencing scheme in η. Figure 2(a) shows the temporal variation of the streamwise component of wall shear ($U_\eta(\eta = 0)$) and the 'displacement thickness' ($\delta^* = [\Phi - \eta\Phi_\eta]_{\eta\to\infty}$) when the two-dimensional solution is perturbed, with $\gamma = -1$ in (3.1) above. This clearly reveals the flow ultimately reverting to the original, two-dimensional state; in this case the crossflow component of wall shear $W_\eta(\eta = 0) \equiv 0$, the flow thereby remaining two-dimensional.

The corresponding results obtained when the amplitude parameter γ is taken to be -5 are shown in figure 2(b). In this case instead of the flow reverting to the original (undisturbed) state, although flow separation seems to occur quite regularly (with $U_\eta(\eta = 0) < 0$), the indications are of a breakdown event, as evidenced in the displacement-thickness temporal development. Further strong evidence of this breakdown is shown in figure 3, in which streamwise velocity profiles ($U(\eta; t)$) are shown, and clearly point to (i) an unbounded increase in this component of the fluid velocity and (ii) a thickening of the boundary layer as the apparent breakdown is approached (in this case at $t = t_s \approx 3.11$), in line with the growth in displacement thickness observed in figure 2(b); intriguingly there is little evidence of singular behaviour of any kind in the vicinity of the wall surface (witness the $U_\eta(\eta = 0)$ distribution in figure 2b).

In the light of the above observations, we now consider the terminal state of the boundary layer as the breakdown time (t_s) is approached. Indeed, this breakdown is of the same class as that found in a related study by Riley & Vasantha (1989), and closely follows the description provided by Banks & Zaturska (1979, 1981), the key features of which resemble the three-dimensional work of Hall, Balakumar & Papageorgiu (1992). In the present case the flow is entirely two-dimensional, and so $\theta \equiv \Psi \equiv 0$. The prominent feature of the breakdown is a thickening of the boundary layer, indicating an inviscid mechanism, and this leads us to the following leading-order behaviours:

$$U = \frac{1}{t_s - t}\hat{U}(\sigma) + \cdots, \tag{3.2}$$

$$\Phi = \frac{1}{(t_s - t)^{3/2}}\hat{\Phi}(\sigma) + \cdots, \tag{3.3}$$

where

$$\sigma = (t_s - t)^{1/2}\eta = O(1), \tag{3.4}$$

Two-dimensional branch	Three-dimensional branch
−1.5186	1.1084
−3.0627	−1.3036
−3.2666	−2.1657
−5.0781	−2.5326

TABLE 1. First four values of the eigenvalue Ω

corresponding to a boundary layer growing in thickness as $(t_s - t)^{-1/2}$. The leading-order equation is then (utilizing $\hat{\Phi}_\sigma = 2\hat{U}$),

$$\hat{\Phi}_{\sigma\sigma}(\hat{\Phi} + \sigma) - 2\hat{\Phi}_\sigma - \hat{\Phi}_\sigma^2 = 0. \tag{3.5}$$

This system is equivalent to that of Banks & Zaturska (1979, 1981), and Hall *et al.* (1992), who showed that a solution to this system exists which, as $\sigma \to 0$, takes the form $\hat{\Phi}(\sigma) \sim (1/3!)\hat{\Phi}_{\sigma\sigma\sigma}(0)\sigma^3$, and thus when $\sigma = O((t_s - t)^{1/2})$, both $\hat{\Phi}$ and $\hat{U}$ become $O(1)$, fully in line with our observations above regarding the fluid in the near-wall region, which does not respond significantly to the flow breakdown mechanisms. There is also a viscous layer in the wall region (which is passive, and of scale $\eta = O(1)$ in the light of our comments above), and another far out in the flow field (located at a finite value of σ, say $\bar{\sigma}$) which serves to blend the inviscid region with the free stream, and is of $O(1)$ thickness, based on the original η scale, but centred at $\eta = \bar{\sigma}(t_s - t)^{-1/2}$.

Two further points of detail are worth making. First, for the class of free-stream perturbation discussed above (i.e. (3.1)), whenever γ was taken to be positive it was found that the flow always ultimately reverted to the original state. Secondly, as discussed above, the flow experienced a breakdown for $\gamma = -5$, but not for $\gamma = -1$; this suggests a threshold amplitude for breakdown, and indeed this was found (numerically) to occur at $\gamma \approx -4.79$.

We now move on to a consideration of the effects of the free-stream perturbation (3.1) on the second $n = 1$ solution, namely the three-dimensional state of Davey & Schofield (1967). The development of the streamwise wall shear stress ($U_\eta\,(\eta = 0)$), crossflow shear stress ($W_\eta\,(\eta = 0)$, in this case the flow is obviously three dimensional), and displacement thickness (δ^*) is shown in figure 4(*a*), for the case $\gamma = 1$. Here the perturbation to the flow does not lead to any breakdown, but neither does it lead to the original three-dimensional state, but rather to the other (two-dimensional) state, pointing to an instability of the former. Indeed, similar calculations were performed, utilizing smaller (but positive) values of γ, and in all cases the ultimate, terminal state was always the two-dimensional one.

The stability of the two states can easily be confirmed, perhaps more conclusively, by taking $n = 1$ in (2.36)–(2.39) above, setting $\tilde{f} \equiv 0$, writing $(\tilde{u}, \tilde{\phi}, \tilde{\psi}, \tilde{\theta}) = (\hat{u}(\eta), \hat{\phi}(\eta), \hat{\psi}(\eta), \hat{\theta}(\eta))\mathrm{e}^{\Omega t}$, and then studying the resulting eigenvalue problem for Ω. The resulting system was solved using second-order central differencing in η, and the eigenvalues were then calculated using first a QZ approach to obtain initial estimates, which were then refined using a local search procedure. The results for the first four eigenvalues for both cases are shown in table 1. The occurrence of a single unstable eigenvalue in the three-dimensional case is clearly seen. There were indeed many (stable) eigenvalues, which appeared to be generally real in nature.

The above procedure is similar to that adopted for limiting corner flows by Ridha (1992), who certainly reported a transition from one (the unstable) state to the other

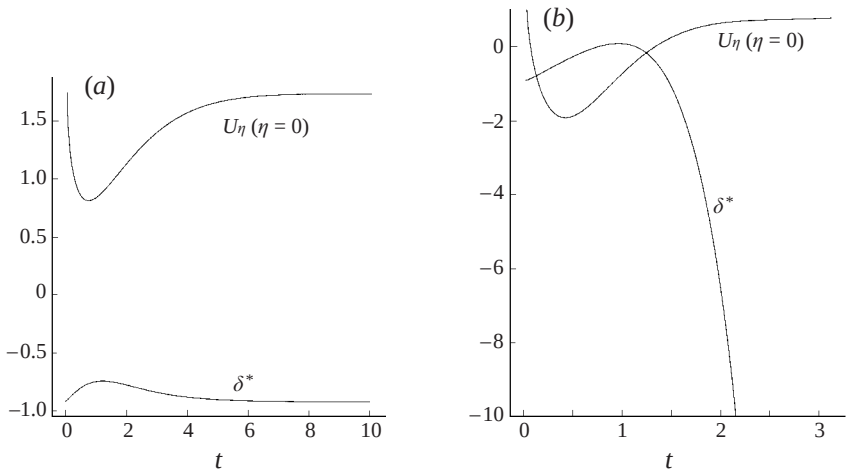

FIGURE 2. Effect of perturbing two-dimensional $n = 1$ base state: (*a*) $\gamma = -1$, (*b*) $\gamma = -5$.

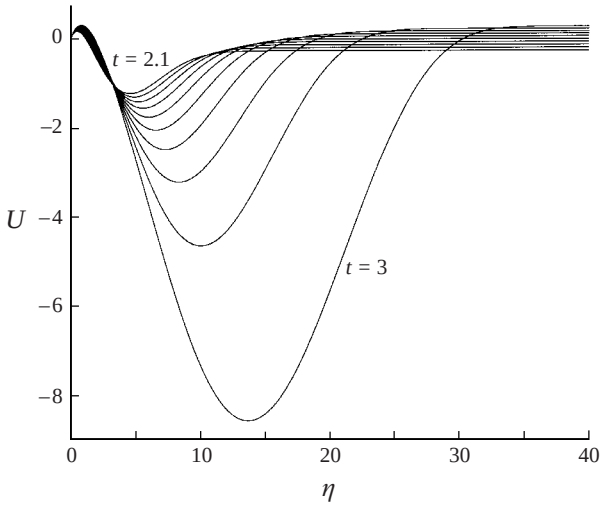

FIGURE 3. Streamwise velocity profiles, two-dimensional $n = 1$ base state ($\gamma = -5$, equal time intervals).

(stable) state also. In that work other values of n were studied (although the solution procedure is then *ad hoc*), but there does seem to be some correlation between base states which exhibit steady leading-edge eigensolutions and the existence of unstable temporal behaviour of this type, with spatial variations ignored. When $n = 1$ other parallels also exist; as noted above, generally just one real and positive value of $(1-n)\lambda$ occurs (and the other, negative values of this quantity are also generally real), and likewise when present, just one real and positive Ω seems to occur (along with many stable and real temporal eigenvalues, i.e. $\Omega < 0$).

We now consider the effect of introducing a perturbation of the form (3.1) with negative γ onto the three-dimensional state. Figure 4(*b*) shows the temporal development of the two wall shear stresses and the displacement thickness when $\gamma = -1$, and

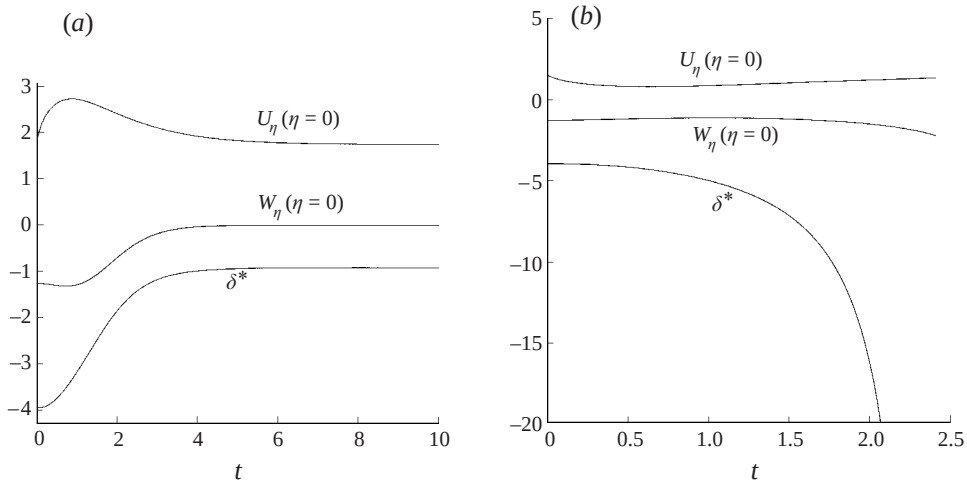

FIGURE 4. Effect of perturbing three-dimensional $n = 1$ base state: (*a*) $\gamma = 1$, (*b*) $\gamma = -1$.

reveals a breakdown at $t = t_s \approx 2.42$, seemingly similar to that encountered with our $\gamma = -5$ calculations on the two-dimensional state. However in figures 5(*a*) and 5(*b*) we show $U(\eta;t)$ and $\Phi(\eta;t)$ profiles, respectively, and these reveal that the streamwise velocity component is apparently bounded as the time of breakdown is approached, whereas the Φ-distribution becomes unbounded.

Intriguingly, it appears that the nature of this breakdown event is related to that described above (in spite of the major differences in the character of the U profiles), and is also a straightforward adaptation of that of Banks & Zaturska (1979, 1981) and Hall *et al.* (1992). In our case, inspection of the governing equations, with the assumption of a predominantly inviscid mechanism, leads us to expect the following leading-order structure:

$$U = \hat{U}(\sigma) + \cdots, \tag{3.6}$$

$$\Phi = \frac{1}{(t_s - t)^{3/2}}\hat{\Phi}(\sigma) + \cdots, \tag{3.7}$$

$$\Psi = \frac{1}{(t_s - t)}\hat{\Psi}(\sigma) + \cdots, \tag{3.8}$$

$$\theta = \frac{1}{(t_s - t)^{1/2}}\hat{\theta}(\sigma) + \cdots, \tag{3.9}$$

where σ is defined (again) by (3.4). Substitution of (3.6)–(3.9) into the governing equations leads us to conclude that

$$\hat{\Psi} = -\hat{\Phi}_\sigma, \tag{3.10}$$

$$\hat{\theta} = \hat{\Psi}_\sigma, \tag{3.11}$$

together with (3.5).

As a final point, other computations were performed using negative values of γ, but of smaller magnitude, and these all ultimately terminated in a singular structure of the type described above.

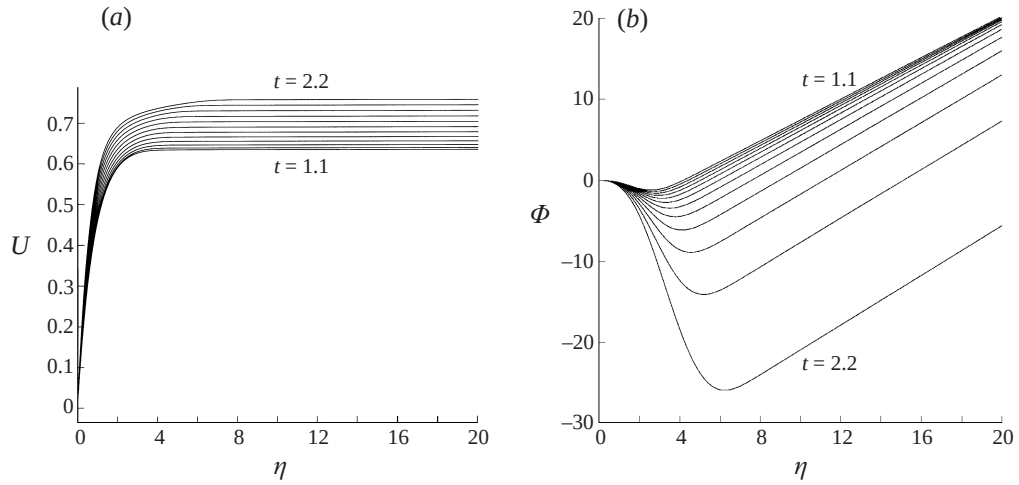

FIGURE 5. Perturbed (*a*) U and (*b*) Φ profiles: three-dimensional $n = 1$ base state, $\gamma = -1$ (equal time intervals)

4. General values of *n*

As noted in § 2, the temporally varying problem in general inevitably leads to a spatially (ξ) varying problem also. We now consider (first) numerical solutions to (2.36)–(2.39) (note from here on we focus our attention exclusively on linearized flow perturbations). These were performed using standard second-order Crank–Nicolson marching procedures in both ξ and t (second-order central finite differencing in η). Figure 6 shows distributions for the streamwise component of perturbation wall shear stress, i.e. $\tilde{\tau} = \tilde{u}_\eta\,(\eta = 0)$ for the $n = 0.35$ two-dimensional (i.e. Falkner-Skan) solution, where a free-stream forcing

$$\tilde{f}(\xi, t) = \xi \mathrm{e}^{-\xi} t \mathrm{e}^{-t} \tag{4.1}$$

has been applied. These results clearly show a temporally and spatially decaying wave-like solution. Note that the perturbation is also two-dimensional in this case and so there is no crossflow component to the flow.

A computation of the corresponding $n = 0.35$ three-dimensional solution, using the same procedure yielded numerically inconsistent solutions. In some ways this is not unexpected, given the existence of steady leading-edge eigensolutions described earlier for this choice of base flow (see figure 1). The case (4.1) was therefore computed using a procedure developed from that of Duck *et al.* (1999) to handle steady flows which possess leading-edge eigensolutions. This scheme involved performing a second-order central finite-difference approximation to (2.36)–(2.39) in the η-direction (using N_η points in the range $0 \leqslant \eta \leqslant \eta_\infty$), together with standard, second-order central differencing in the ξ-direction also; therefore in spite of the system (2.36)–(2.39) being parabolic in nature in ξ, the system was treated as quasi-elliptic in this direction. Initial conditions were imposed at $\xi = 0$ and $t = 0$, namely that

$$\tilde{u}(\eta, 0, t) = \tilde{\phi}(\eta, 0, t) = \tilde{\psi}(\eta, 0, t) = \tilde{\theta}(\eta, 0, t) = 0, \tag{4.2}$$

$$\tilde{u}(\eta, \xi, 0) = \tilde{\phi}(\eta, \xi, 0) = \tilde{\psi}(\eta, \xi, 0) = \tilde{\theta}(\eta, \xi, 0) = 0, \tag{4.3}$$

corresponding to an undisturbed state at the leading edge and initially. Downstream (or rather at a finite location $\xi = \xi_\infty$, suitably far downstream), we imposed Neumann-

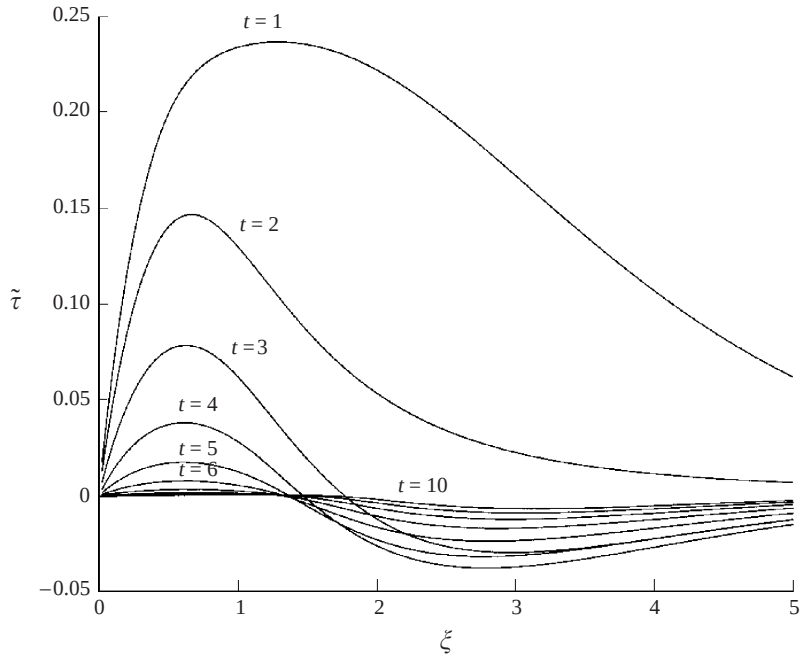

FIGURE 6. Perturbed two-dimensional flow, $n = 0.35$, $\tilde{f}(\xi, t) = \xi e^{-\xi} t e^{-t}$.

type conditions, namely

$$\left.\frac{\partial \tilde{u}}{\partial \xi}\right|_{\xi=\xi_\infty} = \left.\frac{\partial \tilde{\phi}}{\partial \xi}\right|_{\xi=\xi_\infty} = \left.\frac{\partial \tilde{\psi}}{\partial \xi}\right|_{\xi=\xi_\infty} = \left.\frac{\partial \tilde{\theta}}{\partial \xi}\right|_{\xi=\xi_\infty} = 0. \tag{4.4}$$

In the study of Duck *et al.* (1999), it was found that this type of condition proved 'softer', and as a consequence more effective than a Dirichlet-type of condition. N_ξ points were employed in the region $0 \leqslant \xi \leqslant \xi_\infty$. Crank–Nicolson differencing in the timewise direction maintained the overall second-order accuracy of the scheme, but also led to an implicit scheme. Again, following Duck *et al.* (1999), the resulting, entire algebraic system at each timestep may be written symbolically in the form

$$\boldsymbol{A}\boldsymbol{x} = \boldsymbol{R}. \tag{4.5}$$

Here the matrix $\boldsymbol{A}$ may be regarded as a banded matrix, of bandwidth no more than $12 \times N_\xi$ or $12 \times N_\eta$ (depending on equation ordering) by no more than $4 \times N_\xi \times N_\eta$; $\boldsymbol{x}$ denotes the vector-array containing the (unknown) current solution values, and $\boldsymbol{R}$ denotes the vector-array containing forcing terms and values arising from the previous timestep. The overall problem size is about 45% smaller if (2.40) is used in place of (2.38), (2.39), which yields a system with a bandwidth of no more than $9 \times N_\xi$ or $9 \times N_\eta$ by no more than $3 \times N_\xi \times N_\eta$. The sparseness of $\boldsymbol{A}$ was fully exploited in the solution of (4.5) and the ordering of the equations was chosen in order to minimize the size of the stored $\boldsymbol{A}$ array; since the solution is linear, no iteration is required for the unsteady perturbation, and therefore direct solution is possible. A further simplification is that since the elements of the $\boldsymbol{A}$ array are independent of time (merely the timestep Δt), then the inversion of this matrix is only necessary once, leading to a problem at each timestep which only requires simple matrix multiplication.

However, although the results obtained using this method were found to be rea-

sonably independent of time step Δt, they were found to be substantially dependent upon the streamwise grid size $\Delta\xi$. Of particular note was the sharp and temporally increasing distribution close to the leading edge $\xi = 0$; this feature in particular was prone to changes in numerical grids. Unfortunately there were limitations on the number of ξ-points we could consider, since the computational memory requirements can be very significant, even when bandedness is fully exploited. A second, independent computer code was developed independently to solve the system (2.36)–(2.40), which was semi-implicit in time (t) also, but which evaluated the streamwise (ξ) derivatives entirely at the previous timestep. Such an approach leads to a much more compact, banded system than that in (4.5), permitting the usage of a much finer/more extensive grid. However, the results thus obtained were quantitatively similar to those described above, and similar numerical difficulties were experienced.

The question therefore arises as to the nature and causes of these. To investigate (and resolve) these difficulties, in the following section we consider temporally periodic solutions to the system (2.36)–(2.39).

5. Temporally periodic solutions

We seek solutions of the form

$$(\tilde{f}(\xi,t),\ \tilde{u}(\eta,\xi,t),\ \tilde{\phi}(\eta,\xi,t),\ \tilde{\psi}(\eta,\xi,t),\ \tilde{\theta}(\eta,\xi,t)) = \mathrm{e}^{\mathrm{i}\omega t}(\hat{f}(\xi),\ \hat{u}(\eta,\xi),\ \hat{\phi}(\eta,\xi),\ \hat{\psi}(\eta,\xi),\ \hat{\theta}(\eta,\xi)) + \text{c.c.} \quad (5.1)$$

Here ω denotes a real frequency parameter (which we are at liberty to specify), and c.c a complex conjugate. In this case we find it particularly beneficial to exploit (2.40) instead of (2.38) and (2.39), and this leads to the following system for the hatted quantities:

$$\hat{u}_{\eta\eta} + 4n\hat{f} + \xi(1-n)\hat{f}_{\xi} + 2\mathrm{i}\omega\xi^2\hat{f} - 2\mathrm{i}\omega\xi^2\hat{u} + \hat{\phi}U_{0\eta} + \Phi_0\hat{u}_{\eta} - \xi(1-n)U_0\hat{u}_{\xi} - 4nU_0\hat{u} = 0, \quad (5.2)$$

$$2\hat{u} + (1-n)\xi\hat{u}_{\xi} = \hat{\phi}_{\eta} + \hat{\psi}, \quad (5.3)$$

$$\hat{\psi}_{\eta\eta} - 2(1-n^2)U_0\hat{u} + \hat{\phi}\Psi_{0\eta} + \Phi_0\hat{\psi}_{\eta} + 2\Psi_0\hat{\psi} - 2\mathrm{i}\omega\xi^2\hat{\psi} + (n-1)\xi U_0\hat{\psi}_{\xi} = 4n(n-1)\hat{f} - 2\xi^2(1-n)\mathrm{i}\omega\hat{f} - (n-1)^2\xi\hat{f}_{\xi}. \quad (5.4)$$

The boundary conditions to be applied to this system are (2.41)–(2.42), together with (4.2)–(4.4) but with tildes replaced by hats. The resulting system was solved with the free-stream forcing

$$\hat{f}(\xi) = \xi\mathrm{e}^{-\xi}, \quad (5.5)$$

to mirror (4.1).

In the case of base flows which do not possess leading-edge steady eigensolutions, then it is quite clear that standard, parabolic marching schemes (in the ξ-direction) are entirely appropriate. Figure 7 shows results for the streamwise wall stress $\hat{\tau} = \hat{u}_{\eta}$ ($\eta = 0$) for such a case, namely the $n = 0.35$ two-dimensional (i.e. Falkner–Skan) solution, with the frequency parameter ω set equal to unity. Here (and in later figures) we represent the real component of quantities by a solid line, and imaginary components by a dashed line. For this case, on account of the two-dimensional nature of both the base flow and imposed disturbance, there can be no crossflow response. Overall, the flow responds in a fairly damped, unsurprising manner to the free-stream forcing.

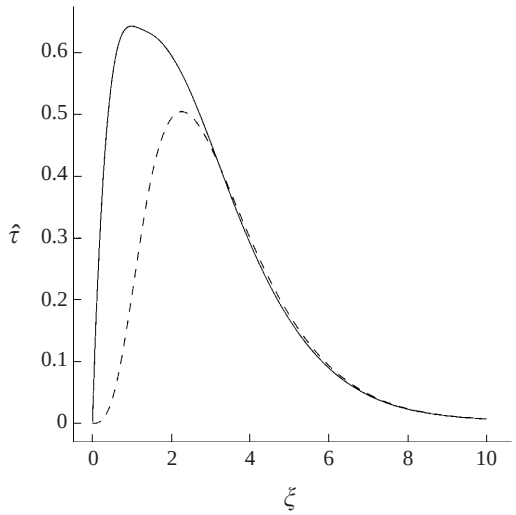

FIGURE 7. $\hat{\tau}$ distributions, $\omega = 1$, $n = 0.35$, two-dimensional base flow.

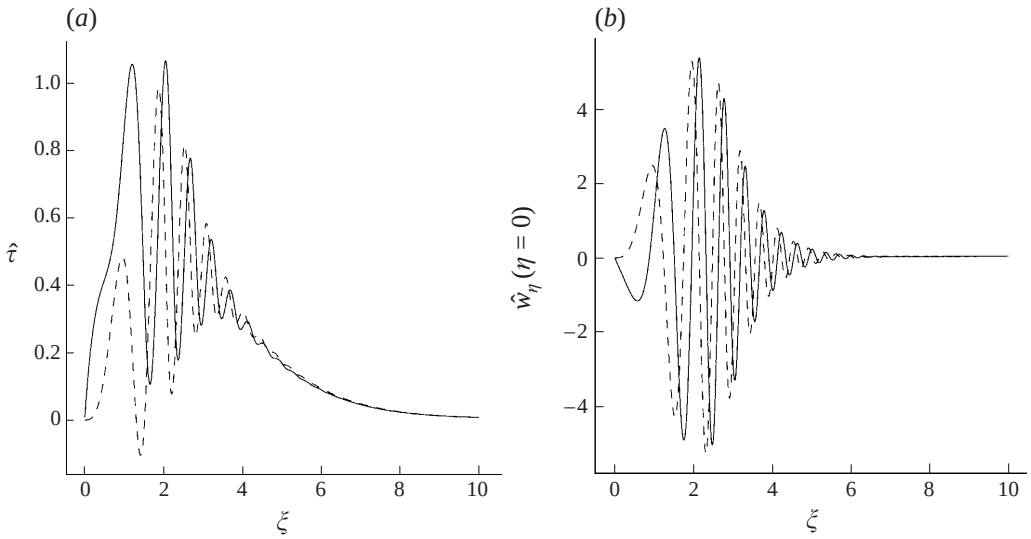

FIGURE 8. (*a*) $\hat{\tau}$ and (*b*) $\hat{w}_\eta\,(\eta = 0)$ distributions, $\omega = 1$, $n = 0.35$, three-dimensional base flow.

Let us now move on to consider base flows which do possess leading-edge steady eigensolutions; we consider again the three-dimensional $n = 0.35$ solution. In figures 8(*a*) and 8(*b*) we show results for the wall shear stresses (streamwise and crossflow, namely $\hat{\tau}$ and $\hat{w}_\eta(\eta = 0, \xi)$, respectively) for the case when $\omega = 1$. The key point to note is that these results were produced using the same, standard (parabolic) marching procedure in the streamwise direction as that used to produce figure 7; it is found that the solution far downstream decays naturally, although there is a significant transient-like growth in the solution at intermediate values of ξ. The response in the wall shear stresses is particularly oscillatory, and of quite sizeable amplitude; the characteristics of the disturbed flow are clearly quite different from those shown in figure 7 for the other base-flow solution.

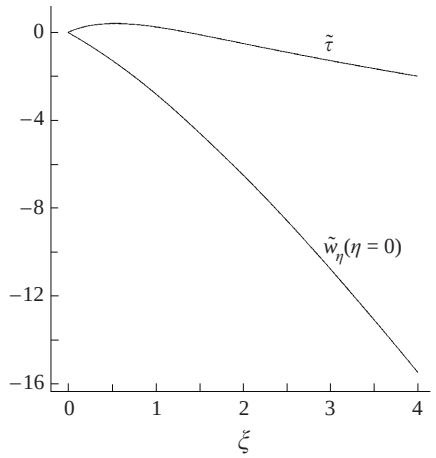

FIGURE 9. $\hat{\tau}$ and $\hat{w}_\eta\,(\eta = 0)$ distributions, $\omega = 0$ (standard parabolic marching scheme), $n = 0.35$, three-dimensional base flow.

For comparison purposes, figure 9 details distributions of $\hat{\tau}$ and $\hat{w}_\eta\,(\eta = 0)$ obtained using the same scheme for a steady, imposed forcing, i.e. when $\omega = 0$; note that here both quantities are entirely real. This case is very different, given that (algebraic) growth is observed downstream; indeed the ξ^λ-type behaviour described in (2.25) is here applicable as $\xi \to \infty$; this type of far-downstream behaviour may be avoided by adding an appropriate multiple of the eigensolution to annihilate it, which may be achieved by imposing far-downstream boundary conditions (i.e. downstream decay), as discussed in § 2. In the case of unsteady flows, currently the main focus of our interest, there seems no reason/need to do this; all unsteady (temporally periodic) flows of this type ultimately decay downstream, albeit after a region of transient growth, which can be significant.

Computations at increasingly higher frequencies (not presented here) clearly indicated the oscillations becoming confined to a region close to the leading edge, whilst computations at lower frequencies indicated the amplitude of both $\hat{\tau}$ and $\hat{w}_\eta\,(\eta = 0)$ increasing (trends that will be confirmed below).

The significant response that can be provoked in these flows (even when the imposed forcing has effectively been removed) suggests the existence of some form of unsteady eigenstate; the known existence of steady eigenstates reinforces this point of view. We note that the transformation

$$\hat{\xi} = \sqrt{\omega}\xi \tag{5.6}$$

leaves the system (5.2)–(5.4) unchanged, but with ω set equal to unity. We then seek to construct a (universal) eigenstate $(\hat{u}_E, \hat{\phi}_E, \hat{\psi}_E, \hat{\theta}_E)$ by solving the system (5.2)–(5.4) with $\omega = 1$, $\hat{f} \equiv 0$, and by triggering the system in some appropriate manner. We adopted a variety of procedures, all of which produced consistent results, although our favoured method was to set $\hat{\phi}_E$ at the outermost grid point in η, at the first $\hat{\xi}$-station away from $\hat{\xi} = 0$, to some small, specified value, say $\hat{\delta}$, and then perform a standard (parabolic) marching procedure downstream, using the condition $\hat{\phi}_{E\eta} \to 0$ as $\eta \to \infty$, consistent with (2.20). In this way the streamwise, free-stream perturbation velocity component is not directly triggered, consistent with $\hat{f}(\xi) = 0$. However, since there was sizeable growth in the solution for $\xi \ll 1$, and because of re-normalization (see below), the particular mechanism for triggering the flow was not important. This type of technique

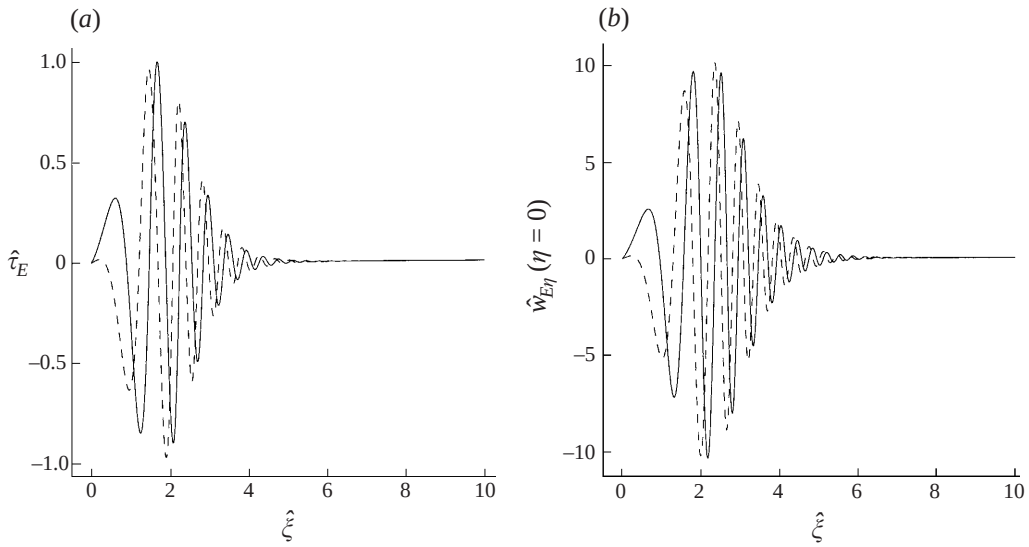

FIGURE 10. (*a*) $\hat{\tau}_E$ and (*b*) $\hat{w}_{E\eta}(\eta = 0)$ (eigenvalue) distributions, $n = 0.35$, three-dimensional base flow.

may be regarded as reminiscent of the 'free interaction' solutions of Stewartson & Williams (1969), and others, linked to early triple-deck work. Figure 10(*a*, *b*) shows the resulting two components of wall shear for this eigenstate, normalized such that the maximum value (amplitude) of $\hat{\tau}_E = \hat{u}_{E\eta}(\eta = 0)$ is unity. Again, just as with the forced (inhomogeneous) results detailed above, after a region of growth away from $\hat{\xi} = 0$, followed by an oscillatory zone, the solution ultimately decays downstream. Of particular note is the not insubstantial amplitude of the crossflow component of wall shear (an order of magnitude greater than the streamwise component). The initial solution growth away from the leading edge may be anticipated, since as ξ (or $\hat{\xi}$) $\to 0$, the system (5.2)–(5.4) becomes quasi-steady, which, from Duck *et al.* (1999, 2000) we know exhibits (steady) spatial growth in eigensolutions. On the other hand as ξ (or $\hat{\xi}$) $\to \infty$, unsteadiness effects undoubtedly play a leading role – the ξ^2 multiplying the unsteady terms in (5.2), (5.4) ensures this. In the Appendix it is shown that sufficiently far downstream, solutions to (5.2)–(5.4) take a form similar to decaying, unsteady eigensolutions found in the context of two-dimensional boundary layers by Lam & Rott (1960), Ackerberg & Phillips (1972) and Goldstein (1983) (these also have some similarity with those found in corresponding axisymmetric boundary layers by Duck 1991). The key result is that the unsteady eigen-behaviour is dominated by a term of the form $e^{-\Lambda\xi^3}$, where Λ is dependent on ω, and is such that $\mathrm{Re}\{\Lambda\} > 0$, irrespective of ω. It is for this reason that downstream decay is assured. One crucial observation here, therefore, is that even an infinitesimal flow perturbation (such as that introduced here, close to $\hat{\xi} = 0$) can provoke a highly significant flow response, suggesting certain ramifications for the boundary-layer transition process in cases when steady leading-edge eigensolutions exist.

A similar treatment, imposing the same form of disturbance as that above on the other (two-dimensional) solution with $n = 0.35$ produced a disturbance which exhibited very rapid decay over just a few streamwise grid points. A final eigenstate we consider is that pertinent to a Blasius base flow. We may anticipate (Luchini 1996; Duck *et al.* 1999) that imposed two-dimensional disturbances (i.e. with no

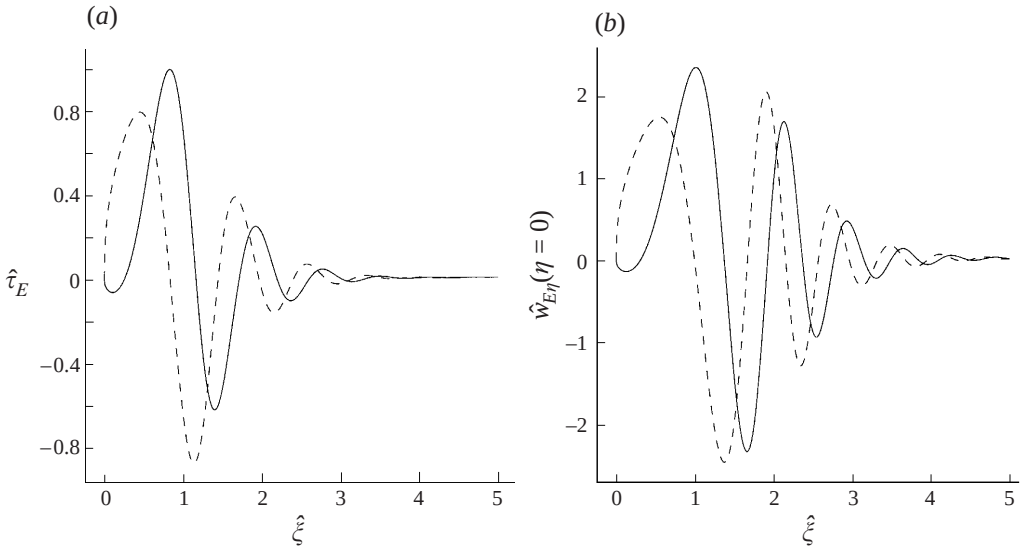

FIGURE 11. (*a*) $\hat{\tau}_E$ and (*b*) $\hat{w}_{E\eta}(\eta = 0)$ (three-dimensional eigenvalue) distributions, Blasius base flow.

crossflow) must be inherently 'stable' (and this was confirmed in our numerical experiments). Therefore we deliberately triggered three-dimensionality, i.e. crossflow, at the first location downstream of the leading edge in our marching scheme, and then proceeded in the usual manner downstream, thereafter. The observed distributions for $\hat{\tau}_E$ and $\hat{w}_{E\eta}(\eta = 0)$ are displayed in figures 11(*a*) and 11(*b*) respectively, where again the distributions have been normalized in such a way that $\hat{\tau}_E$ takes on a maximum value of unity. Again, the eigenstate is predominantly oscillatory in nature; note in particular that the crossflow disturbances are approximately twice those of the streamwise component; the large magnitude of response of the crossflow component, compared with the streamwise component, seems a quite universal feature observed in these eigenfunctions.

The eigenstates just described help explain some of the trends observed in our forced computations, in particular in the limit as $\omega \to 0$, which turns out to be important in understanding some of the results described below. Equation (5.6) indicates a lengthening streamwise scale of $\xi = O(\omega^{-1/2})$ in the low-frequency limit (confirmed by a number of computations performed by the authors). Equally, there is a significant increase in the overall amplitude of the flow response (let us call this A) as $\omega \to 0$. This is quite easy to quantify by supposing $\xi = O(1)$ and $\omega \to 0$ (again), and so from (5.6) $\hat{\xi} \to 0$, in which case the general response to the forcing is likely to be $O(A\hat{\xi}^{\lambda})$, or $O(A\omega^{\lambda/2})$, where λ is that originally introduced in (2.25). This response must be equated to the applied forcing at $\xi = O(1)$ locations, and hence is $O(1)$. We may therefore expect that a measure of the amplitude of the response will be

$$A = O(\omega^{-\lambda/2}). \tag{5.7}$$

Inspection of our numerical results as $\omega \to 0$ indicates this is indeed the case (note that for the three-dimensional $n = 0.35$ case, $\lambda \approx 1.34$).

Above (in § 4) it was shown that an initial value approach to (2.36)–(2.40) failed in the case of basic flows possessing the aforementioned leading-edge eigensolutions. We are now in a position to treat this problem using an alternative approach, based

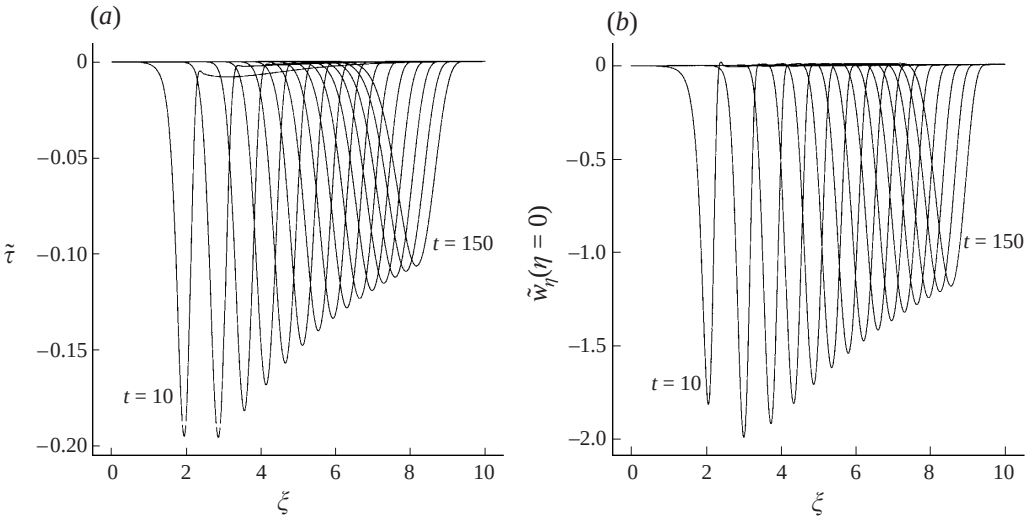

FIGURE 12. (*a*) $\tilde{\tau}$ and (*b*) $\tilde{w}_\eta\,(\eta = 0)$ distributions, three-dimensional base flow, $n = 0.35$, $\tilde{f}(\xi, t) = \xi \mathrm{e}^{-\xi} t \mathrm{e}^{-t}$ (interval 10 time units).

on a (temporal) spectral method. Specifically we consider Fourier transforms, writing

$$(\hat{u}, \hat{\phi}, \hat{\psi}, \hat{\theta}) = \int_{-\infty}^{\infty} (\tilde{u}, \tilde{\phi}, \tilde{\psi}, \tilde{\theta}) \mathrm{e}^{-\mathrm{i}\omega t}\, \mathrm{d}t, \tag{5.8}$$

which leads to the system (5.2)–(5.4) for each ω. For the particular case of the forcing function (4.1), the transform of this is (retaining the above notation)

$$\hat{f}(\xi, \omega) = \frac{\xi \mathrm{e}^{-\xi}}{(1 + \mathrm{i}\omega)^2}. \tag{5.9}$$

The system (5.2)–(5.4), with this forcing, was solved over a range of values of ω (typically $0 \leqslant \omega \leqslant 40$) in steps of $\Delta\omega$ (typically 0.01), each value of ω being considered independently; computations for each value of ω were carried out precisely in the same manner as that described earlier in this section, followed by a quadrature to perform the inversion integral (5.8). Note that since values at $-\omega$ are merely the complex conjugate of those values at $+\omega$ we were able to halve the computational task.

First the computation for the $n = 0.35$ two-dimensional case was repeated, and confirmed the results shown in figure 6. Secondly the corresponding three-dimensional case was tackled using this method, and results for $\tilde{\tau}(\xi, t)$ are shown in figure 12(*a*) and results for the crossflow component of wall shear stress, $\tilde{w}_\eta(\eta = 0, \xi, t)$ are shown in figure 12(*b*). In these figures, results are shown at regular time intervals.

From these results it is clear that there is an initial period of quite substantial growth (until approximately $t = 20$), followed by a gradual decay of the solution in the form of a downstream-convecting wavepacket. It is worth emphasizing here that the applied forcing (4.1) will have decayed away significantly by this peak response time and that it is clear from (5.6) that as time increases, $\xi = O(t^{1/2})$ is the key streamwise scale. It will further be shown in the following section that the wavefront has the (more precise) location $\xi = \sqrt{(1-n)t}$ in this limit. Equally, the (algebraic) decay of the wave with time/ξ may be anticipated from (5.7) above, which leads to the $t \gg 1$ response being $O(t^{(\lambda/2)-1})$; again, detailed study of the above

numerical results revealed consistency with this prediction. This suggests that if $\lambda > 2$ (corresponding to $n > 0.45$ approximately), then this wavepacket must grow as it is convected downstream. We therefore attempted to perform a calculation similar to that performed in the calculation of figure 12(a, b), for $n = 0.5$ (in this case $\lambda = 2.49\ldots$). However, this computation yielded numerical results that were highly dependent on the spatial grid size $\Delta\xi$. Closer inspection of the results revealed that this dependence on $\Delta\xi$ is found in all spectral frequencies ω. On the other hand it was possible to produce consistent, highly accurate eigenfunction distributions (analogous to figure 10a, b) for this larger value of the parameter n. Further careful analysis of the forced (inhomogeneous) results strongly suggested that these had a behaviour of the form $(\Delta\xi)^{\lambda-2}$. This observation points the way to the basic difficulty: our numerical scheme has a truncation error of $O((\Delta\xi)^2)$; the behaviour of the eigenfunction as $\xi \to 0$ is of the form ξ^λ, and this leads to the possible unintentional excitation of the eigenstate occurring when $\lambda > 2$, causing contamination of the solution downstream. The contamination is highly dependent on grid size $\Delta\xi$, hence the overall solution dependence on this quantity. Higher-order differencing schemes are likely to delay this effect, but as λ (and hence n) increases, any finite-difference method based on the above will surely eventually fail.

We experimented with several different numerical procedures (including various transformations in ξ) in a bid to overcome this difficulty, but without success. The fundamental problem is that it is difficult to resolve the two, disparate dependences as $\xi \to 0$ – a linear ξ dependence and a ξ^λ dependence (which we wish to avoid/annihilate).

It was therefore decided to side step this difficulty. As noted above we had no difficulty in generating eigenstates accurately and reliably for cases when $\lambda > 2$. We therefore decided to follow a procedure which triggered the flow perturbation not by means of the free-stream velocity forcing function $f(\xi, t)$, but rather by forcing $\tilde{\phi}(\eta \to \infty, \xi = \Delta\xi, t) = \tilde{\delta}(t)$, mimicking the procedure developed previously to generate eigenstates. More precisely, for each spectral frequency ω we generated the corresponding eigenstate, and then set $\tilde{\delta}(t) = \hat{\delta} t \mathrm{e}^{-t}$, and performed a quadrature of the form (5.8) to invert the solution. Finally a normalization process was undertaken, by which the response was scaled such that the maximum value of $|\hat{\tau}|$ at $t = 1$ was unity. This is of course entirely arbitrary, but does lead to a response which is effectively grid-independent. The results for $\hat{\tau}$ and $\hat{w}_\eta$ ($\eta = 0$) are shown in figures 13(a) and 13(b) respectively. These show the growth/instability of the downstream-moving wavepacket. Indeed this growth was seen to agree well with the argument proposed above, which can be extended to this form of flow excitation, suggesting a wave-amplitude growth of the form $t^{0.249}$ (approximately) as $t \to \infty$; the location of the wavepacket is also described well by the suggestions made earlier.

A further question pertinent to ask at this stage is the reason for the failure of the initial-value approach to the problem, as described in § 4. In particular, there appears to be a failure in the solution linked to the region close to the leading edge. Certainly high-frequency calculations indicated a concentration of the solution close to $\xi = 0$, and (5.6) confirms this will occur as ω increases. Equally, the factor ξ^2 multiplying the time derivatives in (2.36)–(2.40) strongly suggests a subtle behaviour, both spatially and temporally, as $\xi \to 0$. Further, in the light of the difficulties associated with the spectral scheme when $\lambda > 2$, as reported above, one likely scenario for the difficulties with the time-marching procedure described in § 4 is that truncation error is responsible for triggering the algebraic spatial eigenvalue close to $\xi = 0$, and a

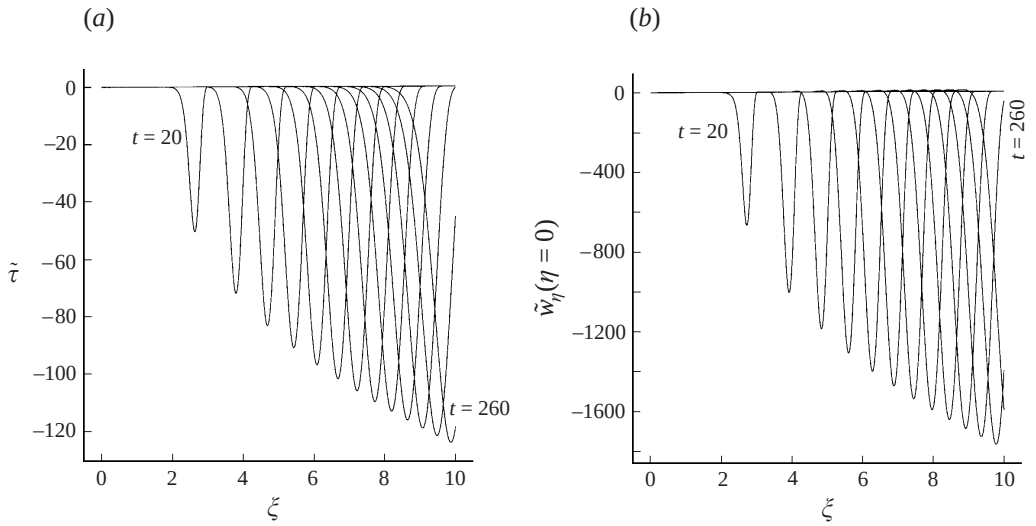

FIGURE 13. (*a*) $\tilde{\tau}$ and (*b*) $\tilde{w}_\eta\,(\eta = 0)$ distributions, three-dimensional base flow, $n = 0.5$, $\tilde{f}(\xi, t) = 0$ (interval 20 time units).

subsequent contamination of the global solution; fortunately the spectral method can bypass these difficulties.

A number of the flow features described above, including the large-time solution, tentatively suggest the combination t/ξ^2 is an important one, and this forms the basis for the next section.

6. Another class of perturbation

The factor ξ^2 which multiplies all time derivatives in (2.36)–(2.40) suggests that we investigate disturbances that, rather than being dependent on ξ, t, (and η), are dependent on ξ, $T = t/\xi^2$ (and η). Accordingly we now regard our tilde variables in (2.31)–(2.35) to be functions of ξ, T and η (rather than of ξ, t and η), which leads to the following set of equations:

$$\tilde{u}_{\eta\eta} + 4n\tilde{f} + \xi(1-n)\tilde{f}_\xi - 2(1-n)T\tilde{f}_T + 2\tilde{f}_T - 2\tilde{u}_T + \tilde{\phi}U_{0\eta} + \Phi_0\tilde{u}_\eta - (1-n)U_0(\xi\tilde{u}_\xi - 2T\tilde{u}_T) - 4nU_0\tilde{u} = 0, \quad (6.1)$$

$$2\tilde{u} + (1-n)(\xi\tilde{u}_\xi - 2T\tilde{u}_T) = \tilde{\phi}_\eta + \tilde{\psi}, \quad (6.2)$$

$$\tilde{\theta} = \tilde{\psi}_\eta, \quad (6.3)$$

$$\tilde{\theta}_{\eta\eta} - 2(1-n^2)(U_0\tilde{u}_\eta + U_{0\eta}\tilde{u}) + \tilde{\phi}\theta_{0\eta} + \Phi_0\tilde{\theta}_\eta + \Psi_0\tilde{\theta} + \tilde{\psi}\theta_0 + 2U_0\tilde{\theta} = (1-n)[-\xi\theta_0\tilde{u}_\xi + 2T\theta_0\tilde{u}_T + \xi U_0\tilde{\theta}_\xi - 2TU_0\tilde{\theta}_T + \xi\tilde{\psi}_\xi U_{0\eta} - 2T\tilde{\psi}_T U_{0\eta}] - 2\tilde{u}\theta_0 + 2\tilde{\theta}_T. \quad (6.4)$$

Note that (6.3) and (6.4) may be replaced by the following (thereby eliminating $\tilde{\theta}$):

$$\tilde{\psi}_{\eta\eta} - 2(1-n^2)U_0\tilde{u} + \Phi_0\tilde{\psi}_\eta + \Psi_{0\eta}\tilde{\phi} - 2\tilde{\psi}_T + 2\Psi_0\tilde{\psi} + (n-1)U_0(\xi\tilde{\psi}_\xi - 2T\tilde{\psi}_T) = 4n(n-1)\tilde{f} - 2(1-n)\tilde{f}_T - (n-1)^2(\xi\tilde{f}_\xi - 2T\tilde{f}_T). \quad (6.5)$$

Setting $n = 1$ in all the above leads to a problem involving merely T and η

dependence, and as such is just the system studied in § 3. At this stage it is worth pointing out certain similarities (and differences) with related work on other problems by previous authors. First, Ridha (1992) performed a class of temporal stability analysis on (limiting forms of) corner boundary-layer flows, equivalent to using the T-variable (as defined above). However, as noted already, he neglected to incorporate the $T(\partial/\partial T)$ term in the system analogous to (6.1)–(6.5) above, which can therefore only be formally correct if $n = 1$. Further, he assumed a solution to be independent of our spatial variable ξ; this in itself is not incorrect, but does restrict the class of flow under consideration. Secondly we note the work on the temporal stability of Jeffrey–Hamel flows by Hamadiche, Scott & Jeandel (1994) and McAlpine & Drazin (1998), who used a temporal variable akin to our T-variable defined above. This variable was also used by Tam (1996) as a basis for studying the non-parallel stability of the Bickley jet.

An interesting point regarding the system (6.1)–(6.5) also worth making is that if the temporal (T) dependence is neglected, i.e. if $|\partial/\partial T| \ll |\partial/\partial\xi|$ the system admits eigensolutions of the spatial form ξ^{λ} (see (2.25)) as $\xi \to 0$. On the other hand if the spatial (ξ) dependence is neglected, i.e. if $|\partial/\partial T| \gg |\partial/\partial\xi|$ then the system seems to admit solutions of the form $T^{-\lambda/2}$ as $T \to \infty$ (same λ as before, with $\mathrm{Re}\{(1-n)\lambda\} > 0$). We therefore see a close linkage between the algebraic spatial behaviour and the corresponding algebraic temporal behaviour.

In order to tackle (6.1)–(6.5) we first make the following transformation:

$$\xi = \mathrm{e}^{s}. \tag{6.6}$$

This renders the problem doubly infinite in s, i.e. $-\infty < s < \infty$ (as $0 < \xi < \infty$), and leads to the advantage of a system of equations whose coefficients are entirely independent of s (or ξ). We next perform a Fourier transform on all variables in the s-direction, as follows:

$$u^{*}(\eta, T; k) = \int_{-\infty}^{\infty} \tilde{u}(s, \eta, T)\mathrm{e}^{-\mathrm{i}ks}\,\mathrm{d}s, \tag{6.7}$$

with obvious definitions for the other starred variables, i.e. ϕ^{*}, ψ^{*}, θ^{*} and f^{*}. The system (6.1)–(6.5) may then be written in the form

$$\begin{aligned} u^{*}_{\eta\eta} + 4nf^{*} + \mathrm{i}k(1-n)f^{*} - 2(1-n)Tf^{*}_{T} + 2f^{*}_{T} - 2u^{*}_{T} + \phi^{*}U_{0\eta} + \Phi_0 u^{*}_{\eta} \\ -(1-n)U_0(\mathrm{i}ku^{*} - 2Tu^{*}_{T}) - 4nU_0u^{*} = 0, \end{aligned} \tag{6.8}$$

$$2u^{*} + (1-n)(\mathrm{i}ku^{*} - 2Tu^{*}_{T}) = \phi^{*}_{\eta} + \psi^{*}, \tag{6.9}$$

$$\theta^{*} = \psi^{*}_{\eta}, \tag{6.10}$$

$$\begin{aligned} \theta^{*}_{\eta\eta} - 2(1-n^2)(U_0u^{*}_{\eta} + U_{0\eta}u^{*}) + \phi^{*}\theta_{0\eta} + \Phi_0\theta^{*}_{\eta} + \Psi_0\theta^{*} + \psi^{*}\theta_0 + 2U_0\theta^{*} \\ = (1-n)(2T\theta_0u^{*}_{T} - \mathrm{i}k\theta_0u^{*} + \mathrm{i}kU_0\theta^{*} - 2TU_0\theta^{*}_{T} + \mathrm{i}k\psi^{*}U_{0\eta} - 2T\psi^{*}_{T}U_{0\eta}) \\ -2u^{*}\theta_0 + 2\theta^{*}_{T}. \end{aligned} \tag{6.11}$$

It was generally found advantageous to replace (6.11) by

$$\begin{aligned} \psi^{*}_{\eta\eta} - 2(1-n^2)U_0u^{*} + \Phi_0\psi^{*}_{\eta} + \Psi_{0\eta}\phi^{*} - 2\psi^{*}_{T} + 2\Psi_0\psi^{*} + (n-1)U_0(\mathrm{i}k\psi^{*} - 2T\psi^{*}_{T}) \\ = 4n(n-1)f^{*} - 2(1-n)f^{*}_{T} - (n-1)^2(\mathrm{i}kf^{*} - 2Tf^{*}_{T}). \end{aligned} \tag{6.12}$$

This type of approach is in the spirit of a number of other boundary-layer

approaches involving the use of Fourier transforms (cf. Burggraf & Duck 1982; Duck & Burggraf 1986; Duck 1985 and others), and frequently simplifies computational procedures in such calculations. In particular, in the system (6.8)–(6.12) above, no spatial (k) derivatives exist, and the problem for each value of wavenumber k can be considered in isolation (at least for this linear class of problem). The primary difficulty with this system, however, is in the T-direction: in particular (6.8), (6.11) and (6.12) all involve a derivative term of the form $[2 - 2T(1-n)U_0]\partial/\partial T$; the coefficient (in square brackets here) will change sign, if $T = ((1-n)U_0)^{-1}$, which is certainly possible. Similar situations have been found to occur in other problems, including the problem of impulsively started flow over a semi-infinite plate (Stewartson 1951, 1973; Hall 1969; Dennis 1972), and also in other problems (Ban & Kuerti 1969; Walker & Dennis 1972; Phillips 1996). Problems involving sign changes of this type are usually referred to as singular parabolic, and are characterized by having regions of mixed mathematical diffusivity with reversals in the direction of convection of vorticity. Such problems obviously require a somewhat different solution approach from standard parabolic problems. It it worth pointing out that this situation is quite different from that encountered in Duck *et al.* (1999), and indeed in §4 above with $\omega = 0$, where the difficulties with parabolic marching procedures were associated with the existence of eigensolutions (rather than changes in the sign of diffusivity). Having said this, we did choose a numerical procedure based on that described in §4. The system (6.8)–(6.11) (or (6.12)) was treated using several distinct approaches. The first was based largely on that described in §4, i.e. the method treated the problem in an elliptic manner, with second-order central differencing in T. As noted already, each value of k may be treated independently, and so for each such value the problem is merely a two-dimensional one (in η and T); standard second-order central differencing was implemented in η. A direct solution procedure was adopted for the solution of the (linear) algebraic system, which was of the general form (4.5); the matrix $\boldsymbol{A}$ is again relatively sparse (banded), and this property was fully exploited. The second method was based on a parabolic marching scheme, in which the direction of differencing in the T-wise direction was determined by the sign of $[1 - (1-n)TU_0(\eta)]$: if this is positive, then the approximation to (6.1) and (6.5) was performed at T levels T_j and $T_j - \Delta T$ (to determine values at $T = T_j$), whilst if $[1 - (1-n)TU_0(\eta)] < 0$, then the difference approximation involves values at T_j and $T_j + \Delta T$ (to determine values at $T = T_j$). Equation (6.2) was tackled using exclusively backward difference approximations, i.e. using values at T_j and $T_j - \Delta T$ to determine the solution at the T_j level. Obviously an iterative approach is necessary here, sweeping repeatedly in T until adequate convergence has been achieved. The method may be regarded as similar to that used by Williams (1975) and Duck, Marshall & Watson (1986). The advantage over the former method (that based on the technique described in §4) is the lower computational memory requirements, the disadvantage being the numerical stability issues related to the iterative process.

As a test case, we took for each k

$$f^*(k, T) = T\mathrm{e}^{-T} \tag{6.13}$$

(cf. (4.1)), i.e. a distribution independent of the spatial wavenumber k, although of course in principle it would be straightforward to use convolution integrals in order to consider more general spatial variations. (6.13) may be interpreted 'physically' as a free-stream perturbation of the particular form

$$\tilde{f} = \xi^{\mathrm{i}k} T\mathrm{e}^{-T} = t\xi^{\mathrm{i}k-2}\mathrm{e}^{-t/\xi^2}, \tag{6.14}$$

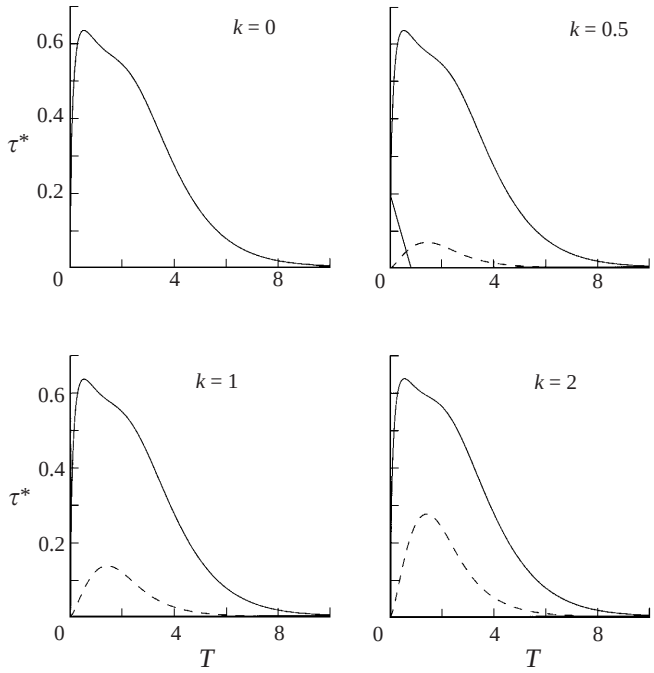

FIGURE 14. τ^* distributions, two-dimensional base flow, $n = 0.35$, $f^*(T;k) = T\mathrm{e}^{-T}$, k as indicated.

wherein k may be regarded as a prescribed parameter, akin to a wavenumber. Our first example relates to the $n = 0.35$ two-dimensional (Falkner–Skan) base flow; to recap, this is an example with no leading-edge eigensolutions. Also, given the two-dimensional nature of the base flow and of the disturbances, then the perturbed flow field is also two-dimensional. Nonetheless the comments above regarding the sign changes of the coefficient of certain of the $\partial/\partial T$ terms are still applicable. For this case, our results were obtained using both the methods outlined above, which produced entirely consistent results. Figure 14 shows distributions of the perturbation streamwise shear stress $\tau^* = u^*_\eta(\eta = 0)$ for selected values of k (here, again we have adopted the convention that real parts are denoted by solid lines, imaginary parts by broken lines). It is clear from these results that in spite of the singular parabolic nature of the system, these results certainly seem to be regular in T. We note too the insensitivity of $\mathrm{Re}\{\tau^*\}$ to k – certainly a small-k expansion suggests that in this limit $\mathrm{Im}\{\tau^*(k)\} = O(k)$ and $\mathrm{Re}\{\tau^*(k)\} = \mathrm{Re}\{\tau^*(k = 0)\} + O(k^2)$, trends that are seem to have applicability over a broad range of k.

We now turn our attention to consider the other base flow solution for $n = 0.35$, i.e. the three-dimensional case. Unfortunately again we encountered a number of numerical difficulties with the two aforementioned procedures. First, a considerably finer numerical grid appeared to be necessary for this class of base flow, and for the direct method described above this led to excessive computational memory requirements (in excess of 2 Gb), rendering the procedure impractical. Secondly the iterative technique, as described above, encountered numerical stability problems, which we were unable to overcome in spite of a good deal of perseverance including considerable amounts of under-relaxation. As a (third) alternative we therefore adopted an approach based largely on that described in § 5. This involved using the Fourier transform scheme in t (i.e. (5.8)). Disturbances corresponding to (6.13) may be transformed into (ξ, ω)-space,

such that

$$\hat{f}(\xi,\omega) = \frac{\xi^{ik+2}}{(1+i\omega\xi^2)^2}, \tag{6.15}$$

where k denotes the wavenumber introduced earlier in this section. Equation (6.15) follows directly by taking the Fourier transform of (6.14) (with respect to t, using (5.8)). For fixed k, the system was then solved in exactly the same manner as that described in the previous section (although in this case it is necessary to consider both positive and negative real values of ω, since the solutions at latter values are no longer the complex conjugates of the former values, except when $k = 0$). The solution was then transformed back to t-space (using (5.8)), divided by ξ^{ik}, and then recast in terms of $T = t/\xi^2$ in order to generate the starred quantities, as in (6.8)–(6.12). As a (partial) check, the results should be invariant in terms of this coordinate, which our results were, except at very early and late times where some degradation was noted (although this was seen to improve with grid refinement). What may be regarded as a more stringent check on the scheme was undertaken by tackling the case for the two-dimensional, $n = 0.35$ base state, and the results thus obtained were entirely consistent with those shown in figure 14. Results for the three-dimensional, $n = 0.35$ base state are shown in figures 15(a) (τ^*) and 15(b) ($w^*_\eta(\eta = 0)$). It is worth mentioning that as the numerical grid was refined, the results using the first (direct) numerical approach described earlier in this section, did appear to be approaching the results shown in figure 15(a, b), although the third (spectral) numerical scheme employed was by far the most feasible.

An important detail to note with the original system (6.8)–(6.12) is that between $0 < T < 1/(1-n)$ the system is entirely parabolic in the forward sense (in T). Beyond $T = 1/(1-n)$ backward parabolicity occurs, initially at the outer edge of the boundary layer, but then, as T increases closer to the surface $\eta = 0$; this applies to both (two- and three-dimensional) classes of flow. As a consequence it is possible to solve the system (6.8)–(6.12) in the zone $0 < T < 1/(1-n)$ using standard parabolic marching procedures, and these yielded a further useful check on our solutions. Hence T-space can be considered to comprise two distinct zones; this observation has important consequences, in particular in understanding/interpreting figures 12 and 13. As time (t) increases, we may identify a definite front to the wavepacket (seen clearly in figures 12 and 13 also), at $T = 1/(1-n)$, or $\xi = \sqrt{(1-n)t}$. Ahead of this location at large times, i.e. $\xi > \sqrt{(1-n)t}$ or ($T < 1/(1-n)$), disturbances will have substantially decayed, leaving the wavepacket behind this front ($\xi < \sqrt{(1-n)t}$).

This effect can be further and convincingly illustrated by performing a numerical experiment based on a very slight modification of the procedure used to compute figure 10. Taking again the $n = 0.35$ three-dimensional base flow, instead of triggering the disturbance ($\hat{\phi}_E(\eta \to \infty) = \hat{\delta}$) close to $\hat{\xi} = 0$, we 'tripped' the flow at locations relatively distant from the leading edge of the plate instead, at $\hat{\xi} = \hat{\xi}_0 > 0$. Figure 16 shows the results for $\hat{\tau}_E$ (the streamwise component of the wall shear) thus obtained, with $\hat{\xi}_0 = 0.5$ and 1; the same normalization process as performed before was used (based on the maximum of $\hat{\tau}_E$). In the case of $\hat{\xi}_0 = 0.5$ the initial input is still amplified downstream, with the maximum amplitude being attained at a location away from the triggering point, i.e. $\hat{\xi} = \hat{\xi}_0$, although inspection of the results reveals significantly less amplification than occurs in figure 10(a). In the case of $\hat{\xi}_0 = 1$ the maximum response is at the triggering point, i.e. $\hat{\xi} = \hat{\xi}_0$, indicating no overall amplification of the initial input, but instead a general oscillatory decay. In view of the observations made above

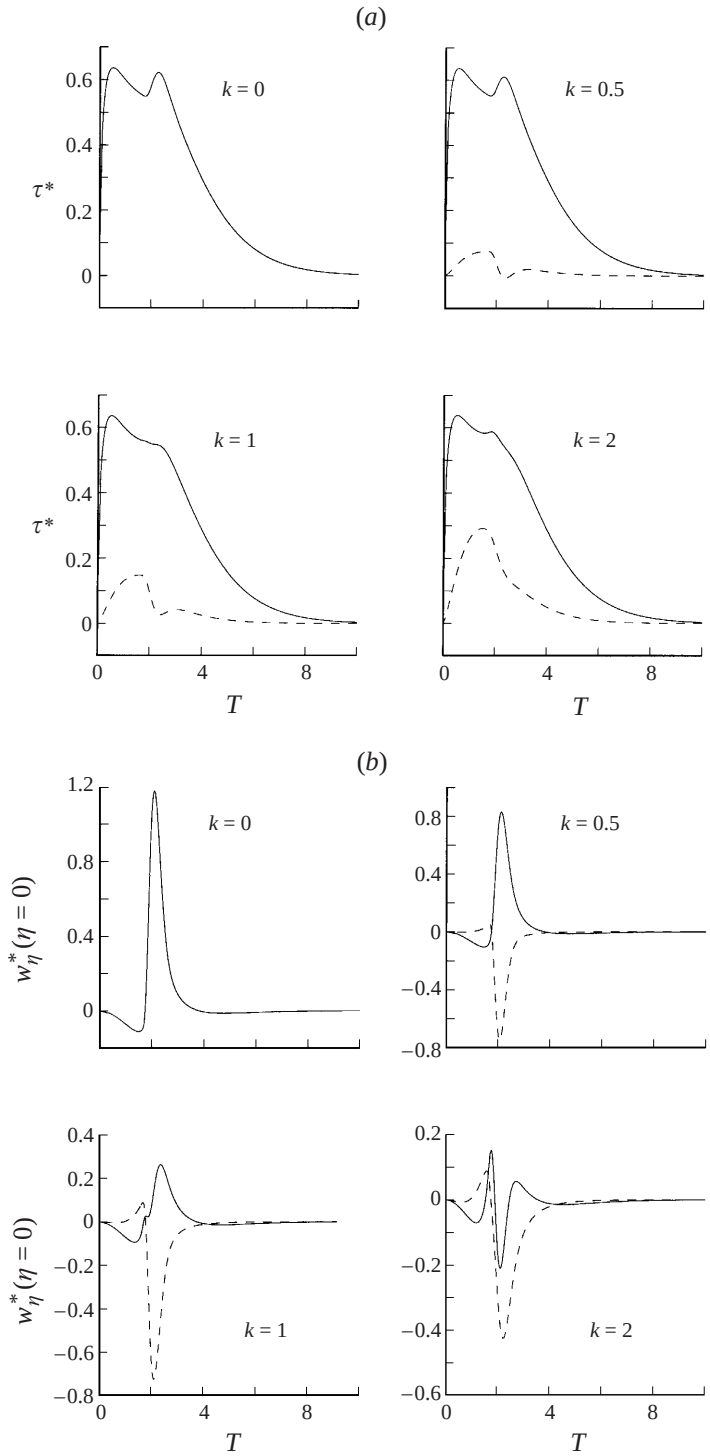

FIGURE 15. (*a*) τ^* and (*b*) $w_\eta^+(\eta = 0)$ distributions, three-dimensional base flow, $n = 0.35$, $f^*(T;k) = T\mathrm{e}^{-T}$, k as indicated.

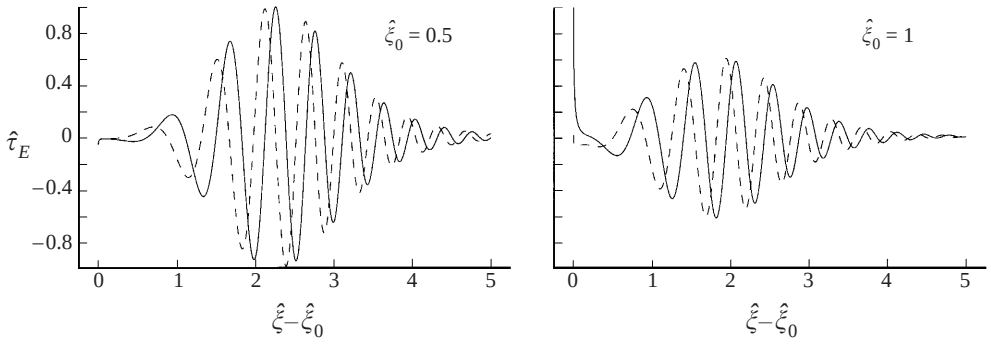

FIGURE 16. $\hat{\tau}_E$ distributions, three-dimensional base flow, $n = 0.35$, $\hat{\xi}_0 = 0.5$, 1.

(and other calculations performed by the authors) we surmise that there exists a critical value of $\hat{\xi}_0 = (1-n)^{1/2}$ beyond which disturbances decay, and ahead of which they will initially grow (although the amplification diminishes with an increase in $\hat{\xi}_0$, the maximum growth being when the disturbance is introduced at the leading edge, namely $\hat{\xi}_0 = 0$), before ultimately decaying sufficiently far downstream. The point $\hat{\xi}_0 = (1-n)^{1/2}$ has some significance, playing a role akin to that of a neutral point.

A question pertinent to ask is the nature of the solution close to the wave front $T = 1/(1-n)$. Here the situation is the same as that for the problem of impulsively started flow past a semi-infinite flat plate; in this case Stewartson (1973) showed that the transition from the Blasius state to the Rayleigh state was accomplished by means of an essential singularity. The analysis of Stewartson (1973) is directly applicable here, in particular the solution involves terms of the form $\exp[-F(\eta)/(T-1/(1-n))]$ for $T > 1/(1-n)$, $|T-1/(1-n)| \ll 1$, $F(\eta) > 0$.

As noted earlier, as $T \to \infty$ the solution will be dominated by a behaviour of the form $T^{-\lambda/2}$ in the case of flows containing leading-edge eigensolutions, otherwise in this limit the flow will be dominated by super-exponentially decaying eigenstates (see the Appendix of Dennis 1972, and we note too the parallels with the Appendix of the present paper).

7. Concluding discussion

In this paper we have identified and investigated a number of aspects of the effect of a class of three-dimensional, unsteady disturbances, as defined in (2.6)–(2.9), that is with a linearly growing crossflow in the crossflow direction, on a base state possessing the same spanwise variation. This form of disturbance has been chosen deliberately, partly to ensure the analysis is completely rational, and also to reduce the dimension of the problem by one (to avoid DNS-type computations – most of our calculations were performed on a laptop computer). It is our view that if a flow is unstable to any reasonable class of disturbance, then probably it will be susceptible to instability in reality. The theory is dependent on the assumption of infinite Reynolds number, and consequently is based entirely upon the (three-dimensional) boundary-layer equations, and as such the theory is based upon completely rational approximations, unlike most traditional stability analyses which require the parallel-flow approximation (for example).

There are several aspects to this study worth emphasizing. Although most of the paper is concerned with linear flow perturbations, most of § 3 is concerned with

fully nonlinear flows. The special choice of $n = 1$ permits much simplification of the disturbance equations, reducing the problem to a two-dimensional one. Whereas the linear stability of the Hiemenz solution is shown (based on our underlying assumptions), a large enough (negative) flow disturbance in the free-stream leads to a nonlinear flow breakdown, of a form related to that of Banks & Zaturska (1979, 1981) and Hall *et al.* (1992), which is predominantly inviscid; there could be some justification in describing this as a form of an early transition process, given its inherent nonlinearity. The picture with the other $n = 1$ solution, namely that found originally by Davey & Schofield (1967) is different. Linear analysis points to instability, which our initial-value approach confirms; a positive 'jolt' of the streamwise velocity in the free stream leads to the flow ultimately becoming Hiemenz-like at large times; a negative 'jolt' leads to a flow breakdown, similar, but not identical, to that observed in the highly perturbed Hiemenz flow situation; the inviscid breakdown structure, and variations thereof, seems a quite generic form of breakdown.

The results of §4, related to the initial-value problem for general values of n (for flows which do exhibit steady, leading-edge eigenstates) are at first puzzling. A variety of numerical procedures was adopted (as described in the text) and all were unsuccessful. However the analysis of §6 sheds some light on these difficulties, in particular because of the significance of the quantity $T = t/\xi^2$; in the (temporal) initial value approach undertaken in §4 it is clear there are likely to be some difficulties in the regime when $t = O(\xi^2)$, wherein there are some subtle variations in the nature of the flow structure, coupled with the existence of flow eigenstates – we believe it is these features that 'conspire' to cause the problems encountered with the numerical procedure of §4. The temporally periodic states, as described in §5, indicate conclusively the possibility of large-amplitude flow responses to quite small flow forcing, due to the excitation of the flow eigenstates. The behaviour seen in figure 11 (together with the eigenvalue distributions shown in figures 10 and 11) mimics results found frequently in non-parallel flow analyses, with an initial regime of growth followed by a (slow) decay (for example this type of behaviour is frequently observed in computations of the parabolized stability equations: Bertolotti 1991; Herbert & Lin 1993). The steady ($\omega = 0$) state is certainly a special case, being the only one with unbounded growth downstream, and as such may be regarded as a singular limit.

It is then fortunate that general temporal variations (as attempted unsuccessfully in §4) are feasible using a Fourier transform method; a wavepacket-type response is seen in these results, and here (again) the behaviour of the flow is controlled, to a large extent, by the magnitude of the steady, spatial eigenvalue λ. Some particularly illuminating results are shown in figures 12 and 13. Figure 12 indicates how a quite small (impulsive) perturbation to the flow can provoke a significant response, which is particularly profound in the crossflow (the maximum amplitude of the forcing, which is applied to the free-stream velocity, is $|\tilde{f}| \approx 0.135$, whilst the component of the wall shear experiences a maximum amplitude approximately 15 times this value). The regime for which $\lambda > 2$ (see figure 16) certainly points to a definite route to transition, given that an impulsive input can trigger an infinite response far downstream/at large time (within the framework of the linear model). Equally, the eigenstates (shown in figures 10 and 11) indicate how an infinitesimal input can provoke a finite flow response. This significant effect will have obvious repercussions for nonlinear studies, where it would appear that solution breakdown (at least within the framework of the boundary-layer formulation), must surely be a strong possibility. Such a failure could then lead to the possibility of a transition process.

Linked to the whole question of 'instabilities' and breakdowns seems to be the physical phenomenon of boundary-layer collisions. Negative crossflow velocities correspond to a flow converging along the line of symmetry ($z = 0$), and certainly base flows of this type are those that do exhibit leading-edge eigenstates, which seem to be at the heart of transient growth. (On the other hand two-dimensional base states, with obviously no crossflow, do exhibit leading-edge eigenstates for $n < 0.167\ldots$.)

The unsteady (temporally periodic) cases, forced over a range of streamwise locations, possess a further subtlety; our computations, performed using the straightforward parabolic marching scheme in ξ clearly yield acceptable decaying solutions downstream. However it is possible to add to these forced solutions an arbitrary multiple of the corresponding eigensolution, to yield an (infinite) family of perfectly acceptable solutions. The resolution of this ambiguity could presumably be achieved through a temporal initial-value type of approach to the problem, although unfortunately none of our numerical schemes permit such an approach under these circumstances (the implication being that the ultimate periodic state is dependent on the time-history of the flow). On a more formal level these solutions as computed in our case are generally the only solutions that are analytic in ξ as $\xi \to 0$, insofar as other solutions would have a component of the form ξ^{λ} in this limit, thus clearly mathematically distinguishing the solutions we have calculated.

There exists a corollary to this paper, which is relevant to the Blasius base flow, and indeed all two-dimensional base states (for which $W_0(\eta) \equiv 0$). In these cases the linearized analysis is equally applicable to crossflow perturbations which do not vary linearly with z, but rather have the following form (with $|\delta| \ll 1$):

$$U^* = x^n[U_0(\eta) + \delta \cos \alpha z \tilde{u}(\eta, \xi, t) + \cdots], \tag{7.1}$$

$$V^* = x^{(n-1)/2}[V_0(\eta) + \delta \cos \alpha z \tilde{v}(\eta, \xi, t) + \cdots], \tag{7.2}$$

$$W^* = \delta x^{n-1}[\sin \alpha z \tilde{w}(\eta, \xi, t) + \cdots]. \tag{7.3}$$

This class of behaviour then has the same crossflow form as that considered in the study of Luchini (1996) on steady perturbations to Blasius flow. The analysis proceeds exactly as before, and it is also possible to renormalize in such a way that we may set $\alpha = 1$ without any loss of generality, and the relevant results in this paper are then directly applicable.

There is an interesting and detailed discussion by Luchini (1996) (who in turn refers to some of the comments of Kachanov 1994) regarding the possible linkage between algebraic growth (at least in the steady context) and bypass transition, to which the reader is referred. We believe the present study adds further evidence for a connection between these two (one theoretical the other experimental) observations. Certainly there do seem to be some intriguing parallels here. Experimentally the bypass phenomenon is generally regarded as being one where there is a rapid nonlinear breakdown (rather than the usual boundary-layer instability mechanism resulting from first the amplification and then the interaction of instability modes). In our results, it is clearly seen that very large flow perturbation amplitudes can be generated, albeit within the confines of linearized theory.

One question posed at the beginning of this paper was linked to the determination of which of the various states found by Dhanak & Duck (1997) and Duck *et al.* (2000) were the most likely to be observed in practice. On the basis of our results regarding the class of disturbances studied here, certainly the suggestion is that it is the state which possesses steady leading-edge eigenvalues with $\lambda < 0$ only that would be the more likely to exist. However we should point out the possibility of other forms

of flow instabilities, not covered by the present study. Obviously the description of the formation of Tollmien–Schlichting waves is not included within this theory and neither is the possibility of crossflow instabilities, both of which are likely occurrences (the latter in flows involving substantial amounts of crossflow).

The authors gratefully acknowledge the support of EPSRC, and a number of useful comments of the referees. P.W.D. wishes to thank Dr S. J. Cowley for reminding him of the work of Banks & Zaturska and Riley & Vasantha.

Appendix

Here we consider the downstream limit of the (homogeneous form of the) system (5.2)–(5.4), having introduced the transformation (5.6) which enables us to set $\omega = 1$ without any loss of generality. Simply stated, we investigate the $\hat{\xi} \to \infty$ form of eigensolutions to this system. The analysis closely follows that of Lam & Rott (1960), Ackerberg & Phillips (1972) and Goldstein (1983) for two-dimensional unsteady disturbances (of infinite wavenumber) to Blasius flow, and of Duck (1991) for the corresponding axisymmetric configuration.

We define a scaled transverse scale corresponding to a thin sublayer as follows:

$$\sigma = \eta\hat{\xi} = O(1) \tag{A 1}$$

in the limit as $\hat{\xi} \to \infty$. We then anticipate that the perturbation (hatted) variables take the following form in this limit:

$$\hat{u} = g(\hat{\xi})\mathrm{e}^{-\lambda\hat{\xi}^3}\hat{u}_1(\sigma) + \cdots, \tag{A 2}$$

$$\hat{\phi} = \hat{\xi}^2 g(\hat{\xi})\mathrm{e}^{-\lambda\hat{\xi}^3}\hat{\phi}_1(\sigma) + \cdots, \tag{A 3}$$

$$\hat{\psi} = \hat{\xi}^3 g(\hat{\xi})\mathrm{e}^{-\lambda\hat{\xi}^3}\hat{\psi}_1(\sigma) + \cdots, \tag{A 4}$$

$$\theta = \hat{\xi}^4 g(\hat{\xi})\mathrm{e}^{-\lambda\hat{\xi}^3}\hat{\theta}_1(\sigma) + \cdots, \tag{A 5}$$

where $g(\hat{\xi}) = o(\mathrm{e}^{\lambda\hat{\xi}^3})$. Note that on the $\sigma = O(1)$ scale,

$$U_0 \sim \frac{\sigma}{\hat{\xi}}U_0'(0), \quad \Phi_0 \sim \frac{\sigma^2}{2\hat{\xi}^2}\Phi_0''(0), \quad \Psi_0 \sim \frac{\sigma}{\hat{\xi}}\Psi_0'(0), \quad \theta \sim \theta_0(0). \tag{A 6}$$

The coefficient in the exponential, namely λ, is as yet undetermined. Substitution of (A 2)–(A 6) into (5.2)–(5.4), utilizing (5.6), taking $\sigma = O(1)$, leads to the following:

$$\hat{u}_{1\sigma\sigma} - 2\mathrm{i}\hat{u}_1 + U_0'(0)\hat{\phi}_1 + 3\lambda(1-n)U_0'(0)\sigma\hat{u}_1 = 0, \tag{A 7}$$

$$\hat{\psi}_1 + \hat{\phi}_{1\sigma} + 3\lambda(1-n)\hat{u}_1 = 0, \tag{A 8}$$

$$\hat{\psi}_{1\sigma\sigma} - 2\mathrm{i}\hat{\psi}_1 + 3\lambda U_0'(0)(1-n)\sigma\hat{\psi}_1 = \hat{K}. \tag{A 9}$$

Combining these equations (and differentiating the result with respect to σ) leads to

$$\hat{\phi}_{1\sigma\sigma\sigma\sigma} + \hat{\phi}_{1\sigma\sigma}\{3(1-n)\lambda U_0'(0)\sigma - 2\mathrm{i}\} = 0. \tag{A 10}$$

Hence, demanding boundedness as $\sigma \to \infty$ leads to the conclusion that

$$\hat{\phi}_{1\hat{\zeta}\hat{\zeta}} = C\mathrm{Ai}(\hat{\zeta}), \tag{A 11}$$

where C is a constant, and

$$\hat{\zeta} = [-3(1-n)\lambda U_0'(0)]^{1/3}\left[\sigma - \frac{2\mathrm{i}}{3(1-n)\lambda U_0'(0)}\right]. \tag{A 12}$$

The boundary conditions on $\sigma = 0$ lead us to impose the condition that $\hat{\phi}_{1\sigma\sigma\sigma}(\sigma = 0) = 0$, and so

$$\mathrm{Ai}'(\hat{\zeta}_0) = 0, \tag{A 13}$$

where

$$\hat{\zeta}_0 = \frac{2\mathrm{i}}{[-3(1-n)\lambda U_0'(0)]^{2/3}}. \tag{A 14}$$

Given that the zeros of the derivative of the Airy function are confined to the negative real axis, we therefore have

$$\hat{\zeta}_0 = \rho_j \mathrm{e}^{\mathrm{i}\pi}, \quad j = 1, 2, \ldots, \infty, \ \ \rho_j > 0, \tag{A 15}$$

and so

$$\lambda_j = \frac{1}{3(1-n)U_0'(0)}\left[\frac{2\mathrm{i}}{\rho_j \mathrm{e}^{\mathrm{i}\pi}}\right]^{3/2}. \tag{A 16}$$

These eigenvalues may be directly correlated with those of Ackerberg & Phillips (1972), and following the arguments proposed by these authors (regarding the proper restriction of the argument of the Airy function to ensure decay), we must have $\arg(\lambda) = -7\pi/4$.

The solution for $\hat{\psi}_1(\sigma)$ can be written

$$\hat{\psi} = B\left[\mathrm{Gi}(\hat{\zeta}) - \frac{\mathrm{Ai}(\hat{\zeta})\mathrm{Gi}(\hat{\zeta}_0)}{\mathrm{Ai}(\hat{\zeta}_0)}\right]. \tag{A 17}$$

The analysis may be continued, with, in general $g(\hat{\xi}) \sim \hat{\xi}^r$ (see Appendix A of Goldstein 1983, and Duck 1991 for an analogous calculation), but the key result here is the super-exponential decay with ξ; the primary difference with the two-dimensional context, however, is the slow (algebraic) decay of $\hat{\psi}_1$ (and hence also $\hat{u}_1$) with σ.

REFERENCES

Ackerberg, R. C. & Phillips, J. H. 1972 The unsteady laminar boundary layer on a semi-infinite flat plate due to small fluctuations in the magnitude of the free stream velocity. *J. Fluid Mech.* **51**, 137.

Andersson, P., Berggren, M. & Henningson, D. S. 1999 Optimal disturbances and bypass transition in boundary layers. *Phys. Fluids* **11**, 134.

Ban, S. D. & Kuerti, G. 1969 The interaction in the boundary layer of a shock tube. *J. Fluid Mech.* **38**, 109.

Banks, W. H. H. & Zaturska, M. B. 1979 The collision of unsteady laminar boundary layers. *J. Engng Maths* **13**, 193.

Banks, W. H. H. & Zaturska, M. B. 1981 The unsteady boundary-layer development on a rotating disc in counter-rotating flow. *Acta Mech.* **38**, 143.

Barry, M. D. J. & Ross, M. A. S. 1970 The flat plate boundary layer. Part 2. The effect of increasing thickness on stability. *J. Fluid Mech.* **43**, 813.

Bertolotti, F. P. 1991 Linear and nonlinear stability of boundary layers with streamwise varying properties. PhD thesis, The Ohio State University.

Bouthier, M. 1972 Stabilitié linéaire des écoulements presque parallèles. *J. Méc* **11**, 599.

Bouthier, M. 1973 Stabilitié linéaire des écoulements presque parallèles. Partie II. La couche limite de Blasius. *J. Méc* **12**, 75.

Brown, S. N. & Stewartson, K. 1975 A non-uniqueness of the hypersonic boundary layer. *Q. J. Mech. Appl. Maths* **28**, 75.

Burggraf, O. R. & Duck, P. W. 1982 Spectral computation of triple-deck flows. In *Proc. Symp. on Numerical Physical Aspects of Aerodynamic Flows*. Springer.

Butler, M. M. & Farrel, B. F. 1992 Three-dimensional optimal perturbation in viscous shear flow. *Phys. Fluids* A **4**, 1637.

Chen, K. K. & Libby, P. A. 1968 Boundary layers with small departures from the Falkner-Skan profile. *J. Fluid Mech.* **33**, 273.

Chen, T. S., Sparrow, E. M. & Tsou, F. K. 1971 The effect of mainflow transverse velocity in linear stability theory. *J. Fluid Mech.* **50**, 741.

Cowley, S. J. & Wu, X. 1994 Asymptotic approaches to transition modelling. In *Progress in Transition Modelling: AGARD Rep.* 793, 1.

Craven, A. H. & Peletier, L. A. 1972 On the uniqueness of solutions of the Falkner-Skan equation. *Mathematika* **19**, 135.

Davey, A. & Schofield, D. 1967 Three-dimensional flow near a two-dimensional stagnation point. *J. Fluid Mech.* **28**, 149.

Dennis, S. C. R. 1972 The motion of a viscous fluid past an impulsively started semi-infinite plate. *J. Inst. Maths. Applics.* **10**, 105.

Dhanak, M. R. & Duck, P. W. 1997 The effects of free stream pressure gradient on a corner boundary layer. *Proc. R. Soc. Lond.* A **453**, 1793.

Duck, P. W. 1985 Laminar flow over unsteady humps: the formation of waves. *J. Fluid Mech.* **160**, 465.

Duck, P. W. 1991 The unsteady laminar boundary layer on an axisymmetric body subject to small-amplitude fluctuations in the free stream velocity. *J. Fluid Mech.* **232**, 415.

Duck, P. W. & Burggraf, O. R. 1986 Spectral solutions for three-dimensional triple-deck flow over surface topography. *J. Fluid Mech.* **162**, 1.

Duck, P. W., Marshall, T. W. & Watson, E. J. 1986. First-passage times for the Uhlenbeck-Ornstein process. *J. Phys.* A: *Maths Gen.* **19**, 3545.

Duck, P. W., Stow, S. R. & Dhanak, M. R. 1999 Non-similarity solutions to the corner boundary-layer equations (and the effects of wall transpiration). *J. Fluid Mech.* **400**, 125.

Duck, P. W., Stow, S. R. & Dhanak, M. R. 2000 Boundary-layer flow along a ridge: alternatives to the Falkner-Skan solutions. *Phil. Trans. R. Soc. Lond.* A **358**, 3075.

Goldstein, M. E. 1983 The evolution of Tollmien-Schlichting waves near a leading edge. *J. Fluid Mech.* **127**, 59.

Hall, M. G. 1969. Boundary layer over an impulsively started flat plate. *Proc. R. Soc. Lond.* A **310**, 401.

Hall, P., Balakumar, P. & Papageorgiu, D. 1992 On a class of unsteady three-dimensional Navier-Stokes solutions relevant to rotating disc flows: threshold amplitudes and finite-time singularities. *J. Fluid Mech.* **238**, 297.

Hamadiche, M., Scott, J. & Jeandel, D. 1994 Temporal stability of Jeffery-Hamel flow. *J. Fluid Mech.* **268**, 71.

Hartree, D. R. 1937 On an equation occurring in Falkner and Skan's approximate treatment of the equations of the boundary layer. *Proc. Camb. Phil. Soc.* **33**, 223.

Herbert, T. & Lin, N. 1993 Studies of boundary-layer receptivity with parabolised stability equations. *AIAA Paper* 93-053.

Hultgren, L. S. & Gustavsson, L. H. 1981 Algebraic growth of disturbances in a laminar boundary layer. *Phys. Fluids* **24**, 1001.

Kachanov, Y. S. 1994 Physical mechanisms of laminar-boundary-layer transition. *Ann. Rev. Fluid Mech.* **26**, 411.

Lam, S. H. & Rott, N. 1960 Theory of linearized time-dependent boundary layers. *Cornell Univ. GSAE Rep.* AFOSR TN-60-1100.

Landahl, M. T. 1980 A note on an algebraic instability of inviscid parallel shear flows. *J. Fluid Mech.* **98**, 243.

Libby, P. A. & Fox, H. 1963 Some perturbation solutions in laminar boundary-layer theory. *J. Fluid Mech.* **17**, 433.

LUCHINI, P. 1996 Reynolds-number-independent instability of the boundary layer over a flat surface. *J. Fluid Mech.* **327**, 101.

LUCHINI, P. 2000 Reynolds-number-independent instability of the boundary layer over a flat surface: optimal perturbations. *J. Fluid Mech.* **404**, 289.

MCALPINE, A. & DRAZIN, P. G. 1998 On the spatio-temporal development of small perturbations of Jeffery-Hamel flows. *Fluid Dyn. Res.* **22**, 123.

MIKHAILOV, V. V., NEILAND, V. YA. & SYCHEV, V. V. 1971 The theory of viscous hypersonic flow. *Ann. Rev. Fluid Mech.* **3**, 371.

NEILAND, V. Y. 1970 Upstream propagation of perturbations in a hypersonic flow with a boundary layer. *Akad. Nauk. SSSR, Izv. Mekh. Zhid. i. Gaza* **4**, 40.

OSKAM, B. & VELDMAN, A. E. P. 1982 Branching of the Falkner-Skan solutions for $\lambda < 0$. *J. Engng Maths* **16**, 295.

PHILLIPS, W. R. C. 1996 On a class of unsteady boundary layers of finite extent. *J. Fluid Mech.* **319**, 151.

REDDY, S. C. & HENNINGSON, D. S. 1993 Energy growth in viscous channel flow. *J. Fluid Mech.* **252**, 57.

RIDHA, A. 1992 On the dual solutions associated with boundary-layer equations in a corner. *J. Engng Maths* **26**, 525.

RILEY, N. & VASANTHA, R. 1989 An unsteady stagnation point flow. *Q. J. Mech. Appl. Maths* **42**, 511.

RIST, U. & FASEL, H. F. 1995 Direct numerical simulation of controlled transition in a flat-plate boundary layer. *J. Fluid Mech.* **298**, 211.

ROSENHEAD, L. 1966 *Laminar Boundary Layers.* Oxford University Press.

RYZHOV, O. S. & ZHUK, V. I. 1980 Internal waves in the boundary layer with the self-induced pressure. *J. Méc.* **19**, 561.

SARIC, W. S. & NAYFEH, A. H. 1975 Nonparallel stability of boundary-layer flows. *Phys. Fluids* **18**, 945.

SCHOFIELD, D. & DAVEY, A. 1967 Dual solutions of the boundary-layer equations at a point of attachment. *J. Fluid Mech.* **30**, 809.

SMITH, F. T. 1979*a* On the nonparallel flow stability of the Blasius boundary layer. *Proc. R. Soc. Lond.* A **366**, 91.

SMITH, F. T. 1979*b* Nonlinear stability of boundary layers for disturbances of various sizes. *Proc. R. Soc. Lond.* A **368**, 573 and **371**, 439.

SQUIRE, H. B. 1933 On the stability of three-dimensional disturbances of viscous flow between parallel walls. *Proc. R. Soc. Lond.* A **142**, 621.

STEWARTSON, K. 1951 On the impulsive motion of a flat plate in a viscous fluid. *Q. J. Mech. Appl. Maths* **4**, 182.

STEWARTSON, K. 1973 On the impulsive motion of a flat plate in a viscous fluid. II. *Q. J. Mech. Appl. Maths* **36**, 144.

STEWARTSON, K. & WILLIAMS, P. G. 1969 Self-induced separation. *Proc. R. Soc. Lond.* A **312**, 181.

TAM, K. K. 1996 Linear stability of the non-parallel Bickley jet. *Can. Appl. Maths Q.* **3**, 99.

TERENT'EV, E. D. 1978 On an unsteady boundary layer with self-induced pressure in the vicinity of a vibrating wall in a supersonic flow. *Dokl. Akad. Nauk SSSR* **240**, 1046.

TREFETHEN, L. N., TREFETHEN, A. E., REDDY, S. C. & DRISCOLL, T. A. 1993 Hydrodynamic stability without eigenvalues. *Science* **261**, 578.

WALKER, J. D. A. & DENNIS, S. C. R. 1972 The boundary layer in a shock tube. *J. Fluid Mech.* **56**, 19.

WILLIAMS, P. G. 1975 A reverse flow computation in the theory of self-induced separation. *Proc. 4th Intl Conf. Num. Meths in Fluid Dyn.* Lecture Notes in Physics, vol. 35 (ed. R. D. Richtmyer), p. 445. Springer.

ZHUK, V. I. & RYZHOV, O. S. 1978 On one property of the linearized boundary-layer equations with a self-induced pressure. *Dokl. Akad. Nauk SSSR* **240**, 1042.